

**Impact of Immersed Conductive Objects and Relative Influence of Immersion
Depth on Quasi-Steady Burning Behavior of Dodecane Fuel Slick on
Turbulent Waters**

By

Mahesh Shankar Kottalgi

A Thesis

Submitted to the Faculty

of

WORCESTER POLYTECHNIC INSTITUTE

in partial fulfillment of the requirements for the

Degree of Master of Science

in

Fire Protection Engineering

March 2023

Approved:

Professor Ali S. Rangwala, Advisor
Worcester Polytechnic Institute,

Dr. Sharanya Nair, Co Advisor
Worcester Polytechnic Institute

Professor Albert Simeoni, Dept Head, Committee Member
Worcester Polytechnic Institute

Abstract

With the increase in industrialization, activities in the modern world predominantly have revolved around the usage of liquid/ fossil fuels for transportation and energy requirements directly or indirectly. A large percentage of these fossil fuel needs are accommodated by offshore drilling. These drilling methods and subsequent oil transport used for offshore oil rigs increase the risk of accidental release of fuel into water bodies. Oil contamination can create a hazard to life and property. In-situ burning (ISB) is one of the spill response techniques in practice, where the spill area is subjected to a controlled ignition and burned till extinguishment [4-8]. Although ISB is an effective countermeasure to burn fuel spills, understanding the burning behavior of fuel under wavy water conditions is necessary to increase the effectiveness of the overall burn. To understand the heat transfer mechanism for a fuel layer burning in ocean conditions, an experimental platform is used to simulate wavy water surfaces. Furthermore, the study investigates the influence of turbulent water and the immersed conductive object on the steady burning behavior of a fuel layer floating on a turbulent water surface.

To systematically investigate the effect of turbulence, an experimental platform simulating free surface turbulence is created using a submerged axisymmetric jet pointing upwards, the result is an isotropic regime in the horizontal plane with the free bulk flow for experimenting. The corresponding turbulence created lies in the range of 0 cm/s to 4.2 cm/s. For Phase-I of the study, a 5 mm fuel slick is used to study turbulence as a parameter for the experiments. Results show a change in turbulent boundary conditions causes an increase in heat extraction from the bottom of the fuel layer, thereby reducing the mass burning

rate by 45 % at a turbulent intensity of $u' = 4.2$ cm/s, along with a decline in overall flame height compared to no turbulence case. A model developed to predict the heat transfer coefficient at the fuel-water interface shows the heat transfer coefficient value (h) dominates as a result of internal mixing with the increase in turbulence.

For Chapter 3, based on the studies in Chapter 2, an intermediate turbulence intensity equal to 1.7 cm/s comparable to water turbulence in a calm ocean is chosen for the experiments. To improve the burning under the turbulent water sublayer condition, a 10 mm diameter copper conductive object is immersed at different depths in the fuel. The copper rod collects the flame's heat and transmits it into the fuel layer via conduction, thereby increasing the burning rate by more than 1.4 times. A heat transfer model shows that the case with a small rod immersion depth (~10 mm) in a 40 mm fuel layer is best at improving burning because the heat losses from the object to the water sublayer are the lowest. The model also shows that the heat from the flame transmitted by the rod is primarily distributed in a region close to the surface of the fuel, where nucleate boiling around the rod surface dominates. As more of the rod is immersed in the fuel layer, the heat dissipation to the turbulent water increases nearly five times, thereby reducing the nucleation sites around the rod surface and the burning rate. The implications of burning fuel slicks during in-situ burning in turbulent water conditions are espoused.

Acknowledgments

Several people have contributed to the successful completion of this research. I express my sincere gratitude to my Advisor, Prof. Ali S. Rangwala, for his kindness and honest guidance. His support throughout my academic and non-academic career at Worcester Polytechnic Institute has been a beam of light. I would like to thank my Co Advisor, Dr. Sharanya Nair for guiding me in every step of this research. Her Patience and knowledge with directing me through this journey has helped me complete this work. I am sincerely grateful to Prof. Albert Simeoni, Head of Department and thesis committee member for his assistance and constant support without whom this degree would not come to fruition. I thank the Bureau of Safety and Environmental Enforcement (BSEE) and Karen Stone for the research motivation and encouragement for taking up this novel research. My sincere gratitude towards all the professors and staff whom I have worked with and taught me during my stay here at WPI.

I thank Kemal, Matt, Nate, Chuming, Li, Hamed, Ray, Fritz, Veronica, Pi, Suhas, Andy, Rayna; my friends and colleagues who made my stay at Combustion Lab and Fire lab memorable.

Lastly, I would like to thank my parents and my siblings for their constant encouragement for all things I have done in my life. I would not have come this far without the love and support of my family, and I am eternally indebted.

Table of Contents

Abstract.....	1
Acknowledgments	3
List of Figures.....	6
List of Tables	7
Nomenclature	8
Chapter 1: Introduction	9
1.1. Early Research-----	9
1.2. Recent Research-----	10
1.3. Immersed Conductive Objects -----	11
1.4. Current Research Objective -----	12
Chapter 2: Influence of water turbulence on burning behavior of dodecane fuel slick	14
2.1. Preface -----	14
2.2. Experimental Setup -----	14
2.3. Effect of Turbulence on Burning Behavior (Transient) -----	17
2.4. Analysis of Turbulence on Burning Behavior (Quasi-steady) -----	19
2.4.1. Quasi Steady State Region-----	21
2.4.2. Transient Burn-----	25
2.5. Conclusion -----	29

Chapter 3: Influence of Immersed Conductive Objects on Quasi-Steady Burning Behavior of Fuel Slick in Turbulent Waters.....	31
3.1. Preface -----	31
3.2. Experimental Methodology -----	31
3.3. Results and Discussion-----	36
3.3.1. Effect of Rod Depth -----	36
3.3.2. Heat Transfer Mechanism -----	40
3.4. Conclusion -----	48
Chapter 4: Conclusion and Future Work.....	50
References.....	52

List of Figures

Figure 2.1. Schematic diagram of the experimental platform with instrumentation and fire pool dimensions; inset images show thermocouple locations in gas, fuel, and water phases.-----	15
Figure 2.2. Experimental platform for fuel burning on wavy water with continuous fuel feeding setup. -	16
Figure 2.3. Fuel slick thickness (δ) for four cases (Baseline $u' = 0$ cm/s, $u' = 1.7$ cm/s, $u' = 3.3$ cm/s, $u' = 4.2$ cm/s) is shown as a function of time and corresponding burn efficiencies for the respective cases.-----	19
Figure 2.4. Temperature evolution with time for 5 mm fuel slick with a turbulence intensity of $u' = 1.7$ cm/s.-----	20
Figure 2.5. Photographs at 90 seconds into quasi-steady state burning of 5 mm n-dodecane fuel layer showing flame heights with increasing turbulence intensity. Cases showed at (a) $u' = 0$ (still water layer), (b) $u' = 1.7$ cm/s, (c) $u' = 3.3$ cm/s, and (d) $u' = 4.2$ cm/s.-----	21
Figure 2.6. Fuel-air interface showing energy terms used for heat transfer model analysis.-----	22
Figure 2.7. Energy input from the flame [$qs (+)$], and net total energy available for fuel vaporization [mLF] terms obtained using thermocouple data for n-dodecane fuel burning as a function of turbulent intensity (u').-----	24
Figure 2.8. Calculated burning rate from the heat transfer model in comparison to the experimental burning rate obtained directly from the fuel replenishing system for baseline and three turbulent intensities (u').-----	25
Figure 2.9. In-depth temperature in the fuel vs. relative position of the thermocouples comparing a). baseline – no turbulence case and b). worst- turbulence case ($u' = 4.2$ cm/s).-----	26
Figure 2.10. Comparison of the predicted and experimental values for fuel-water interface temperature (T_{δ}) as a function of time-----	28
Figure 2.11. Calculated heat transfer coefficient values as a function of turbulence intensity (Baseline - $u' = 0$ cm/s $u' = 1.7$ cm/s, $u' = 3.3$ cm/s, $u' = 4.2$ cm/s). The value of h is obtained by minimum error analysis.-----	29
Figure 3.1. Schematic diagram of the experimental platform for fuel burning on wavy water with continuous fuel feeding setup and an immersed rod; inset images show thermocouple locations on the rod surface; and in gas, fuel, and water phases.-----	32
Figure 2.2. Experimental platform for fuel burning on wavy water with continuous fuel feeding setup and an immersed rod.-----	33
Figure 3.3 Mass loss rate plotted against time to show progression of burning across the experiment for baseline case.-----	35

Figure 3.4. Images of baseline case with fuel level marked and measured at 30, 60, 90, and 120 seconds into achieving quasi-steady state.----- 36

Figure 3.5. Mass loss rate of the burning fuel as a function of rod depth for 5 mm, 10 mm (rod immersed close to fuel surface), 20 mm, 30 mm (rod partially immersed in fuel), and 50 mm (rod immersed in fuel and water). Error bars presented with a standard deviation of three repeated experiments. ----- 37

Figure 3.6. Photographs at 90 seconds into quasi-steady state burning of 40 mm n-dodecane fuel layer showing flame heights at the turbulence of $u' = 1.7$ cm/s. Cases showed at rod depths: (a) 10 mm, (b) 30 mm, (c) 50 mm, and (d) baseline (no rod). ----- 38

Figure 3.7. Time evolution of 50 mm rod experiment at turbulent intensity $u' = 1.7$ cm/s marked with a defined steady-state region. (a) shows temperatures in the gas phase, and (b) shows temperatures in the rod. ----- 39

Figure 3.8. Control Volume (red dash Line) showing heat energy terms for the cases. (a) Copper rod immersed across the entire depth of fuel and partially in the water, (b) Copper rod immersed in fuel layer above the water sublayer, and (c) Baseline - no rod case. ----- 41

Figure 3.9. Energy budgeting chart showing the energy terms: energy input [qs (+), qr (+), $qrod$ (+)], energy loss [$qrod, loss$ (-), $qw, loss$ (-)], and overall energy available for fuel heating and vaporization [$m(LF + Cp\Delta T)$]; Obtained using thermocouple data for n-dodecane fuel burning under the turbulent intensity of $u' = 1.7$ cm/s.----- 44

Figure 3.10. Obtained heat transfer model results (a) Energy loss to water sublayer plotted against baseline and three rod depths, (b) Additional mass loss rate due to immersed rod plotted against rod depths, (c) Calculated burning rate from the heat transfer model for 12 trials in comparison to the experimental burning rate obtained directly from the fuel replenishing system for baseline and three immersion depths, (d) Calculated and experimental MLR for baseline and three immersion depths. (B^* denotes baseline case).----- 47

Figure 3.11. Thermal penetration depth (δ) observed indicated by bubbling sites on the rod surface with 30 mm depth and 10 mm rod depth.----- 48

List of Tables

Table 2.1. Experimental summary with turbulence and the observed regression rates for the corresponding tests 18

Nomenclature

A_{pool}	Area of the fire pool (m ²)
A_F	Area of the fuel surface (m ²)
A_{rod}	Cross-sectional area of the rod (m ²)
C_p	Specific heat of fuel (J/kg K)
D	Diameter of the pool (m)
d_r	Diameter of the rod (m)
k_{air}	Thermal conductivity of the air (W/m K)
k_{rod}	Thermal conductivity of the copper (W/m K)
k_{fuel}	Thermal conductivity of the fuel (W/m K)
k_{water}	Thermal conductivity of the water (W/m K)
L_F	Heat of gasification of fuel
\dot{m}	Mass burning rate of fuel (g/min)
$\dot{q}_s (+)$	Energy input from the gas phase to the fuel surface (W)
$\dot{q}_{rod (+)}$	Heat conducted through the rod to the liquid layers (W)
$\dot{q}_{rod,loss (-)}$	Heat loss to the water layer from the rod (W)
$\dot{q}_{w,loss (-)}$	Heat lost from the fuel to the water layer (W)
$\dot{q}_r (+)$	Radiative heat feedback from the gas phase to the fuel surface (W)
ΔT	Change in temperature during sensible heating (°C)
t	Time to reach a steady state (s)
u'	Turbulence intensity (root-mean-square velocity) (cm/s)
ρ	Density of fuel (Kg/m ³)
α	Thermal diffusivity of the fuel (m ² /s)
δ	Thermal penetration depth (m)
ε	Emissivity at the surface of the liquid layer
σ	Stephan Boltzmann constant (W/m ² k ⁴)
T_g	Average temperature above the fuel surface in the gas phase (K)
T_b	Surface temperature of the liquid pool (K).

Chapter 1: Introduction

In recent years, oil spills have been in the spotlight for their devastating effects on life and property. With progressive demand and dependability on fossil fuels, spills accidents are more probable than ever before [1]. In the US, a 24,696-gallon spill was detected originating from an underwater pipe on the southern coast of California in 2021 [2]. On an international stage, the coastlines of Peru in 2022 saw a major spill disaster with 10,000 barrels of crude oil spewed into the Pacific Ocean. The spill covered an area of 40 square miles destroying protected marine ecosystems and livelihoods depending on it [3]. Thompson et al. [4] first analyzed the practical aspects of using in-situ burning as a spill mitigation tool, the process involves gathering and burning the spilled oil in open waters; Goodier and Siclari [5] further investigated to conclude in-situ burning as a means of reducing the release of oil to the environment. Over the years, In-situ burning (ISB) is identified as an accepted strategy for responding to oil spills on water bodies, [6-9], The response rate to these spills plays a pivotal role in minimizing the environmental impacts of these spills [10]. As ISB gains its attention as an effective countermeasure because of its ease of operation and deployment, studies underlying the dynamics of burning with real-case ocean scenarios become crucial for its successful operation.

1.1.Early Research

Early experimental research related to ISB focused on fuels burning on a static water sublayer to deduce thermal models for their distinctive burning behavior. The direction of the research was driven toward analyzing the independent parameters associated with ISB operations. Buist [11] and Arai et al. [12-13] observed critical thickness as an important parameter for successful ISB operation. Oil layers thinner than critical thickness lost heat to the water sublayer causing early extension or boilover. Initial research focused extensively on the boilover phenomenon and showed that the intensity of boilover is associated with fuel layer thickness and burn area [14-16]. Garo et al [17-20] extended the research to evaluate the cause of boilover at a macro scale, showing surface tension forces greatly affect the intensity of nucleation sites in the water sublayer that causes the boilover phenomenon. The following study developed a 1-D conduction

heat conduction model, to compare in-depth temperature distribution. Arai et al [21] further studied the effect of burn area on the boilover of the liquid. He studied three burn pool diameters, 48 mm, 98 mm, and 203 mm, and showed that for smaller pool fires at 48 mm diameter, the temperature values in the fuel decrease and the gradient across the fuel layer become negligible when the water starts to boil under the fuel layer. On the contrary, the pool fires at 98 and 203-mm diameter, the gradient in the fuel increases, and the burning rate increases at boilover. Ito et al. [22] and Inamura et al [23] studied hydrocarbon fuels to analyze in-depth temperatures at the liquid-fuel interface and found Rayleigh convection generated near the fuel surface increased the convective heat transfer from the fuel interface by 30%. Van Gelderen et al. [24] further showed that in order to improve ISB, fuel slick thickness plays an important role and that the regression rate, average mass loss rate, and burn efficiency decreased with a slick thickness of less than 10-20 mm with most heat lost to the water sublayer.

1.2.Recent Research

While previous research was driven toward small-scale studies focusing on parameters affecting ISB operations, more recent studies have explored aspects of ISB operations that are scalable. Such study with Van Gelderen et al. [25] developed a laboratory-scale large water-to-oil ratio experimental platform called Crude oil Flammability apparatus (COFA), the platform was used to study the burning efficiency and its dependency on the observed size in in-situ burning conditions. Three alkaline fuels (n-octane, dodecane, and hexadecane), a mixture of alkaline (1:1:1 volumetric ratio), and two crude oil fuels (light and medium-light) were compared resulting in a model to derive realistic water-oil heat transfer boundary conditions. Kong et al. [26] studied the influence of the wind on the overall burn efficiency and flame drag it has on burning crude oil fuel on the water. The study resulted in a model predicting flame base drag for pool fires in open water. All the research mentioned in literature above were done so in an environment where only the fuel is allowed to regress over time or a fuel floating on a static water sublayer regressed over time. Further research in recent times has evolved to slightly different avenues of ISB operations. Sauer et al. [27-28] examined the interaction of waves and the burning behavior of a regressing dodecane and kerosene

fuel using a paddle-type wave simulator setup done with a 10 cm diameter fire pool. Results demonstrated that an increase in the wave intensity leads to reduction of the overall burning behavior. Similarly, Chang and Rangwala [29] investigated the influence of surface turbulence on a floating fuel slick using an axisymmetric upward-pointing jet configuration. The experiments were done with crude oil as fuel with a 10 cm diameter burn pool. The experiments showed a strong correlation between turbulence and burning behavior with decreasing burn rates at higher turbulence. Aurell et al. [30] also saw similar results while examining emissions from crude oil burns with waves and varied boom configurations.

1.3. Immersed Conductive Objects

Literature reviews show an underlying commonality pointed out in the studies from previous researchers which is a thermal boundary condition in which the heat loss from the fuel layer to the water sublayer is a major factor in reduced burning. Given this, the concept of increasing the burn efficiency by enhancing thermal feedback to the fuel with the introduction of an immersed conductive object called Flame Refluxer™ (FR) has been proposed in recent years [31-35]. The process involves introducing an object of high thermal conductivity in the fuel layer, where the upper region of the object exposed to the flame named the ‘collector region’, collects heat from the flame and conducts it to the lower region of the object immersed in the fuel layer named ‘heater region’. This heat feedback ensures pre-heating and vaporization of the fuel thus enhancing the burn. The concept of FR technology has been experimentally studied and validated by varying dimensions, materials, and the number of immersed objects [32-34]. Consequently, the studies reported a significant increase in mass burning rates due to the established secondary thermal loop. Based on the experimental data from the literature, Nair et al. [35] developed a predictive model to analyze the effect of the object material, dimensions, and fuel properties on pool fire burning. Pi et al. [36] further investigated ethanol pool fires with an aluminum disk immersed in the fuel and reported growth in nucleation sites with the presence of an aluminum disk and also reported a direct correlation between the disk diameter and increased mass burning rate. Using the concept of immersed conductive objects and metal meshes, Sezer et al. [37-38] further developed a computational model to predict the mass loss rate of pool

fires. Most of the aforementioned work relies on optimizing the thermal properties and dimensions of the immersed objects for maximum heat input to the fuel layer. The present work thus explores further into the in-situ burn application that has a moving water sublayer under the fuel layer. The cooling effect of water thus affects the heating path from collector to heater and subsequently to the fuel. Additionally, in such a scenario, it can also be realized that heater section will have varied heat losses based on the intensity of the water sublayer motion. This forms a major motivation for the study where the effect of wavy water is initially analyzed at a lab scale and then a study on the effect of the proximity of the heater section to the water is carried out.

1.4.Current Research Objective

While newer studies are venturing into lesser-explored aspects of ISB [31-38], no studies have been performed exploring both turbulence and enhancing burn behavior of fuel slick as a coupled parameter. Remarkably, only a handful of studies have examined the effect of surface turbulence and waves on the burning behavior of the fuel. While surface turbulence in nature is driven by wind, water surface currents, and geographical terrains [39], studies integrating the effects of turbulence intensity on the performance of the burning fuel slick and providing a quantitative explanation are scarce.

Thus, the current research paves a platform to understand the influence of turbulence on the fuel slick floating on the water sublayer. This is particularly interesting because of direct applications for controlled ISB operations; hence the current study focuses on examining and analyzing the heat transfer boundary condition at the fuel-water interface in the presence of turbulence. The study further extends the research parameter to analyze a known immersed object in a quantified turbulent field as opposed to a stagnant water layer along with a steady layer of fuel replenished continuously to achieve a quasi-steady state, unlike previous studies. The research dives into examining the effect of the depth of an immersed copper rod in the presence of a wavy water sublayer and investigating the burning behavior of fuel as a consequent effect. A quasi-steady burning state approach additionally ensures the heat transfer mechanisms

in the hot gas phase, and the fuel and water layers can be analyzed independently of any transience in the burning system.

The global objective of this work is to advance the in-situ burning technique by using Flame Refluxer™ technology by defining the optimal operating conditions for a wavy water condition. The specific objectives of the work are as given below:

1. Investigate the effect of turbulence on the burning behavior of the thin fuel slick regressing with time.
2. Investigate the heat transfer boundary condition under the influence of turbulence with a fuel slick that is maintained steady at a certain fuel thickness.
3. Investigating an optimal condition (immersion depth) with an immersed conductive object that will enhance the overall burning rate.
4. Develop a heat transfer model to quantify the energy input and loss values to understand the variation in fuel slick burning for cases:
 - (a) with varying turbulence of water sublayer
 - (b) with and without immersed object (with turbulence)

Chapter 2: Influence of water turbulence on burning behavior of dodecane fuel slick

2.1. Preface

Understanding the effect of water turbulence on the mass burning rates of fuel slicks is the first phase of the study. The experimental platform designed for quasi-steady burning of fuel slick on turbulent water is presented. Using the setup, the influence of the turbulence intensity on the mass burning rates is reported and the heat transfer mechanism is analyzed using energy balance at the fuel-air interface. The study then progresses into quantifying the heat transfer coefficient.

2.2. Experimental Setup

Figure 2.1 and 2.2., show the schematic of the modified experimental platform used in the study originally designed and developed by Chang and Rangwala [29]. A cylindrical Pyrex glass of 100 mm inner diameter sits inside a 5 mm thick 200 mm × 200 mm square polycarbonate tank that is 350 mm tall. The second polycarbonate enclosure around the 100 mm glass cylinder is to provide a cooling bath surrounding the burn pan. A 12.7 mm diameter jet nozzle located in the center of the setup sits 5 mm above the bottom of the containment setup. Two axisymmetric ports placed adjacent to the main inlet jet are used to recirculate the water creating a closed-loop system. Studies show the turbulent velocity components in vertical and horizontal directions become consistent in a horizontal plane at a height three times the confinement diameter [40-45]. Hence, the velocity fluctuation in the region of interest becomes directly proportional to the flow rate of the pump and can be controlled using a flow valve. Furthermore, the experimental platform in the previous studies validated that the turbulence in the region of interest used for the experiments is isotropic [29]. A centrifugal pump (Little giant magnetic drive pump) rated to handle a flow rate of 0 to 15 liters/min is used to create turbulence. The corresponding root mean square of velocity fluctuations (u'_{rms} denoted as u' in the study) at the confined region ranges from 0 (no turbulence case) to 6.6 cm/s (turbulence case - Highest) for the setup. Continuous feeding of fuel is arranged using a Wensuijia portable single-channel syringe pump with a feed rate of 0.0013 g/min to 18.81 g/min for 60 ml syringes to

maintain a constant fuel level above the water surface. This ensures a quasi-steady burning of the fuel above the water; the total volume of fuel is enough to reach the quasi-steady state burning stage where the flame behaviors and mass loss rates are captured.

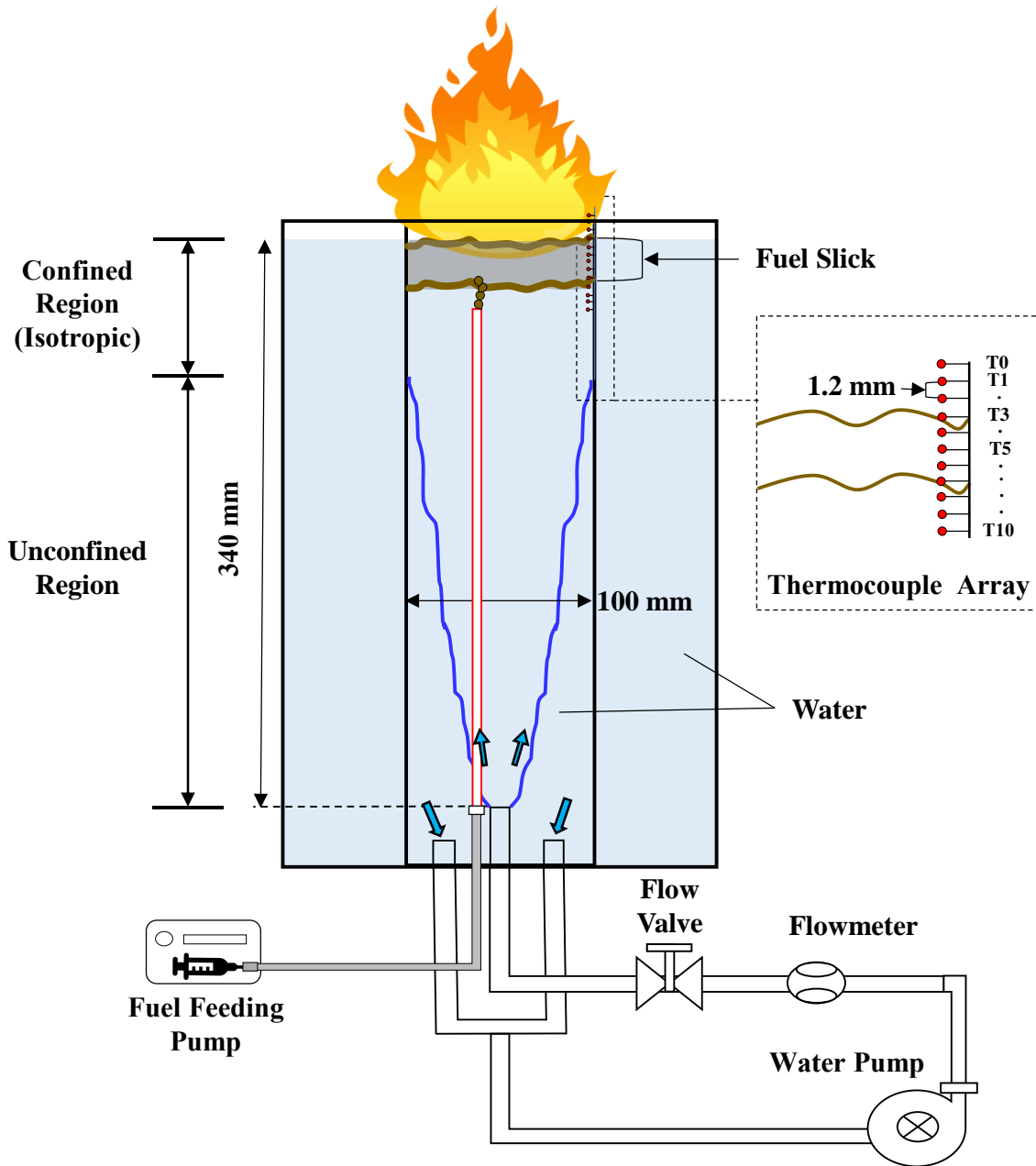


Figure 2.1. Schematic diagram of the experimental platform with instrumentation and fire pool dimensions; inset images show thermocouple locations in gas, fuel, and water phases.

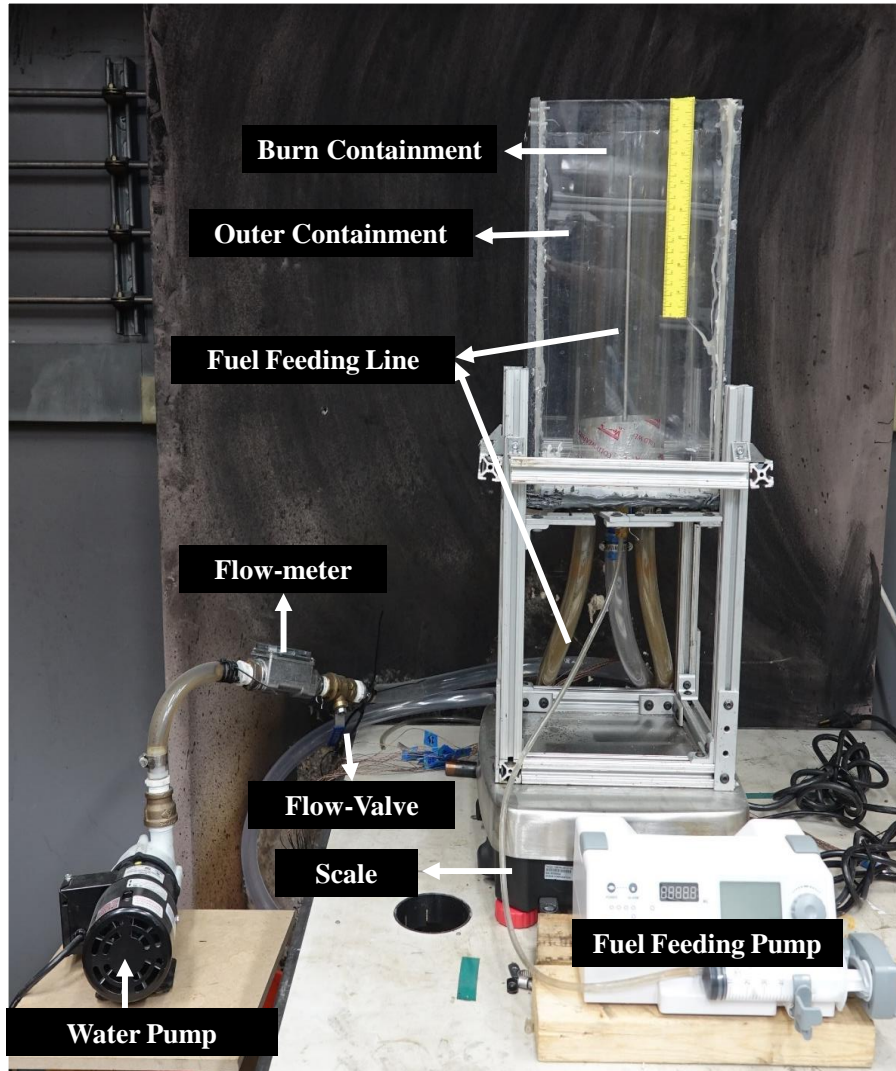


Figure 2.2. Experimental platform for fuel burning on wavy water with continuous fuel feeding setup.

In this study, experiments are performed using n-dodecane, typically used as a surrogate for crude oil burns due to its similar boiling point and well-defined thermo-physical properties of this single-component fuel [46]. The initial fuel slick thickness and ullage are maintained at 5 mm and 10 mm, respectively across all tests. The measured density of liquid n-dodecane is 752.2 kg/m^3 . A thermocouple array consisting of 11 omega K-type 36-Gauge thermocouples is carefully placed 1.2 mm apart in the inner cylinder to measure water, fuel, and gas phase temperatures precisely as shown in Figure 2.1. Data from the thermocouples are sampled at a frequency of 1 Hz for all experiments. N-dodecane for these

experiments has the following properties [22, 46]: boiling point = 216 °C, density ($\rho = 752.2 \text{ kg/m}^3$), specific heat ($C_p = 2.2 \text{ J/g K}$), thermal conductivity ($k = 0.2 \text{ W/m K}$), thermal coefficient of volumetric expansion ($\beta = 9.9 \times 10^{-4} \text{ K}^{-1}$), kinematic viscosity ($\nu = 1.36 \times 10^{-6} \text{ m}^2/\text{s}$), and thermal diffusivity ($\alpha = 1.21 \times 10^{-7} \text{ m}^2/\text{s}$).

Turbulence cases are tested for intensities with the fluctuating velocity component (u') ranging from 0 cm/s to 5.0 cm/s. For the experiments, the containment chambers are filled with water, and the pump is initiated to achieve a set flow rate ($u' = 0$ to 5.0 cm/s) using a flow valve. The setup is allowed to run idle for 10 minutes to stabilize the flow to the chamber and eliminate any air in the flow tube. Once the set flow is achieved, fuel is poured in from the top which corresponds to 5 mm by weight (29.54 g). Measurements from the thermocouple are collected using NI LabVIEW software. A Sony Exmor R handycam is used to record the flames. Each of the cases was repeated three times for repeatability. For the experiments, instantaneous flame heights are measured using an open-source software 'ImageJ', where a reference length measurement is identified for calibration. This reference length scale is converted into a pixel scale to obtain pixels/cm. This known Pixel-length relationship is used to obtain the visible continuous flame heights in the study.

2.3.Effect of Turbulence on Burning Behavior (Transient)

The first half of the experiments is performed to understand the effect of turbulence on the overall burning behavior of the fuel slick. For this reason, transient experiments are conducted with turbulence cases starting with $u' = 0.8 \text{ cm/s}$ as the smallest turbulence case and incremented gradually until a turbulent condition is reached where ignition is not sustainable. It is observed that for a 5 mm fuel slick, the flames do not sustain beyond $u' = 4.2 \text{ cm/s}$ (Highest turbulence case). An initial fuel slick measuring 5 mm in thickness is ensured at the start of the experiment and allowed to burn until self-extinction. Oil residue after the burn is collected using a 3M oil-only absorbent pad [47] to quantify the burning efficiency. A global regression rate is calculated by subtracting the residue from the initial mass of oil and dividing it by the duration of the burn. Table. 2.1 shows the regression rate of the fuel for varied turbulence cases along with a baseline no-turbulence case for benchmarking. It is seen that the overall regression rate decreased as the

intensity of the turbulence progressed. This is due to the cooling effect from the water turbulence under the fuel layer. The burning rate reduces by 18% from 2.95 g/min for the baseline ($u' = 0$ cm/s) case to 2.56 g/min for the $u' = 1.7$ cm/s turbulence case. And for the highest turbulence case at $u' = 4.2$ cm/s, the burn rate declines to 1.74 g/min showing a reduction of 44% from the baseline case. Thus, the mass loss rate shows that turbulence intensity plays a major role in the burning of fuel slicks.

Table 2.1. Experimental summary with turbulence and the observed regression rates for the corresponding tests

Turbulence - u' (cm/s)	Fuel left post-burn (g)	Mass loss rate - Global \dot{m}_G (g/min)	Burn Efficiency
0	1.7	2.95	94.3%
0.8	6.7	2.61	77.6%
1.7	6.8	2.56	77.4%
2.5	7.4	2.48	75.7%
3.3	7.5	2.25	75.5%
4.2	15.2	1.74	49.0%
5.0	No Ignition	No Ignition	No Ignition

Figure 2.3., shows the averaged estimation of reduction in the fuel slick thickness (δ) for four cases (Baseline $u' = 0$ cm/s, $u' = 1.7$ cm/s, $u' = 3.3$ cm/s, $u' = 4.2$ cm/s) as a function of time, obtained from average regression rate data. The burning efficiency is the highest for the baseline case with 94% of the fuel burned until self-extinction. Only 0.29 mm of fuel was left as residue at end of the burn for the baseline case seen in Figure 2.3. However, about 2.55 mm of fuel residue was left for the highest turbulence case at $u' = 4.2$ cm/s in this study. While the burn durations were about 500 s for all cases, the burn efficiency dropped to 49% for the highest turbulence case ($u' = 4.2$ cm/s) as compared to the baseline ($u' = 0$ cm/s) case. This clearly shows the reduction in the burning rates with turbulence and subsequent reduction in burn

efficiency as well. Further, these transient tests portray the values of mass burning rates with turbulence that will be useful while setting the fuel feed rates in the continuous feeding tests.

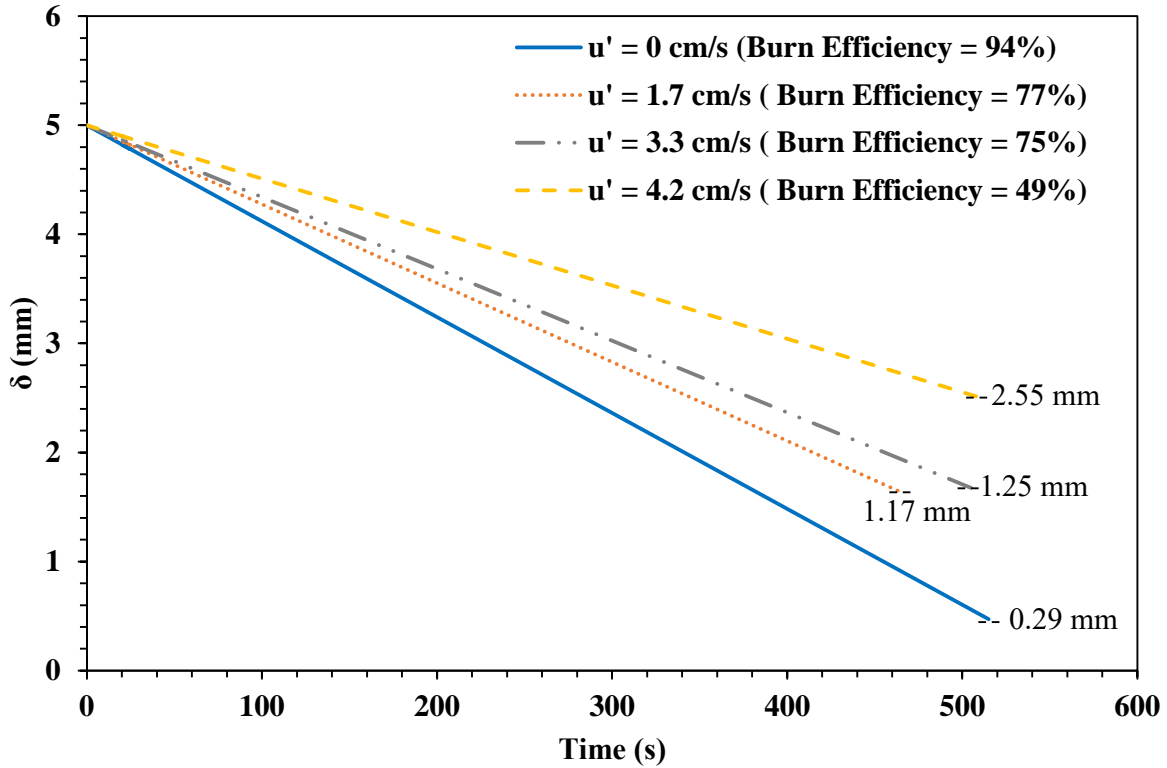


Figure 2.3. Fuel slick thickness (δ) for four cases (Baseline $u' = 0$ cm/s, $u' = 1.7$ cm/s, $u' = 3.3$ cm/s, $u' = 4.2$ cm/s) is shown as a function of time and corresponding burn efficiencies for the respective cases.

2.4. Analysis of Turbulence on Burning Behavior (Quasi-steady)

For ISB burns it is seen that a layer of oil is collected to a desired thickness and ignited, and the thickness is relatively maintained until it regresses over time and extinguishes once a critical thickness is achieved. To better understand the ISB operation conditions and heat transfer mechanism involved, a test matrix is designed to study the same for this phase using quasi-steady experiments to decouple the transience in the burn behaviour. Considering this, the same slick thickness of 5 mm is chosen for the experiments. The initial layer of fuel once ignited is maintained at 5 mm thickness until a condition is reached where fuel burned in the system is equal to fuel fed, this condition is referred to as quasi-steady state for this study.

This quasi-steady state is held for roughly 300 s before the fuel supply is cut off and the remaining fuel is allowed to burn until it self-extinguishes. Experiments with three turbulence cases ($u' = 1.7$ cm/s, 3.3 cm/s and 4.2 cm/s respectively) along with a non-turbulence case are considered for this study.

Figure 2.4. shows the time evolution of an experiment with a baseline case for 5 mm fuel slick without the presence of turbulence. The temperatures in the gas phase, and liquid phases until extinction are shown. The thermocouples sampled at 1 data point/second (1 Hz) are averaged at 15-second intervals to smoothen and reduce the noise in the data. The region circled in black, where the temperatures spike is the ignition of the fuel at $t = 30$ seconds. The fuel feeding is maintained until the system is in equilibrium shown in red. This is also the region where the variation in the temperature gradient in the gas phase is less than 10%. At this stage, the region marked in red shows a steady state where the temperature fluctuations are minimal. Fuel is cut at $t = 500$ seconds and the remaining fuel is left to burn until self-extinction at $t = 900$ s. The region in green shows a transient stage where the temperatures increase as a result of regressing fuel.

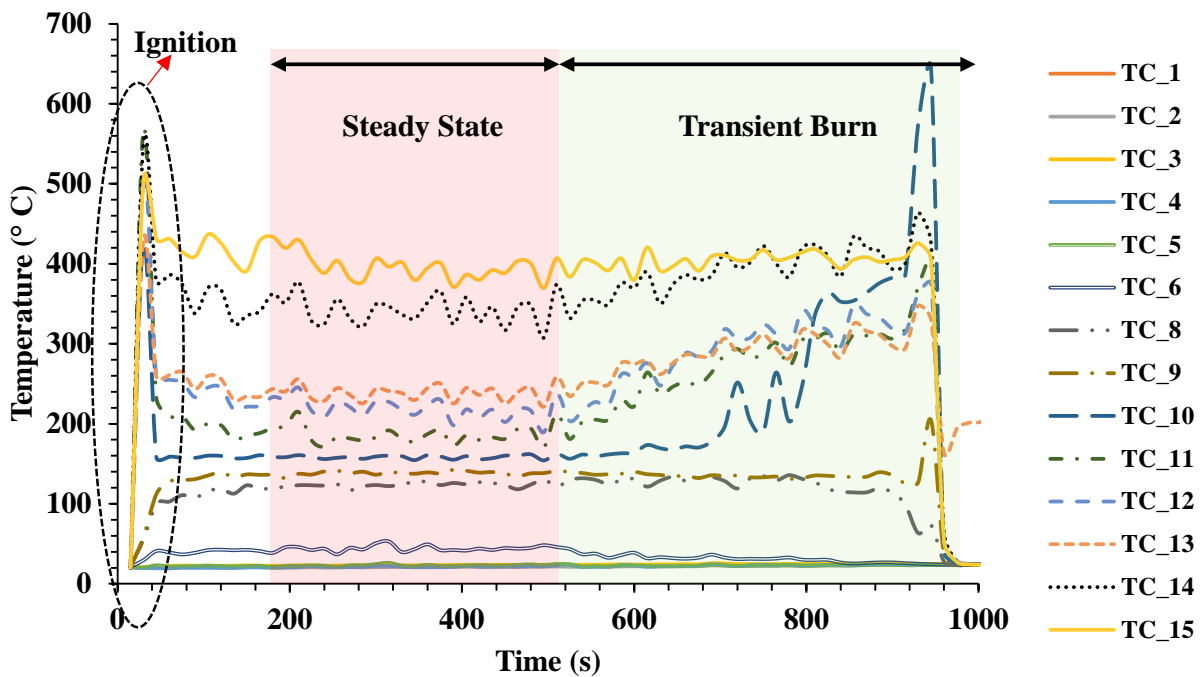


Figure 2.4. Temperature evolution with time for 5 mm fuel slick with a turbulence intensity of $u' = 1.7$ cm/s.

2.4.1. Quasi Steady State Region

Figure 2.5. shows the comparison of flame photographs at different turbulent intensities. It is seen that the flame heights reduce from 27 cm for no turbulence case to 12 cm with the highest turbulence case tested, owing to low burning rates of the fuel as turbulence increases. The corresponding mass burning rates decrease monotonically from 4.4 g/min for the no turbulence case (still water layer) to 2.3 g/min for the high turbulence case tested. The burning rates shown in Figure 2.5. are directly obtained from the feed rate of the fuel pump to maintain a quasi-steady state condition.

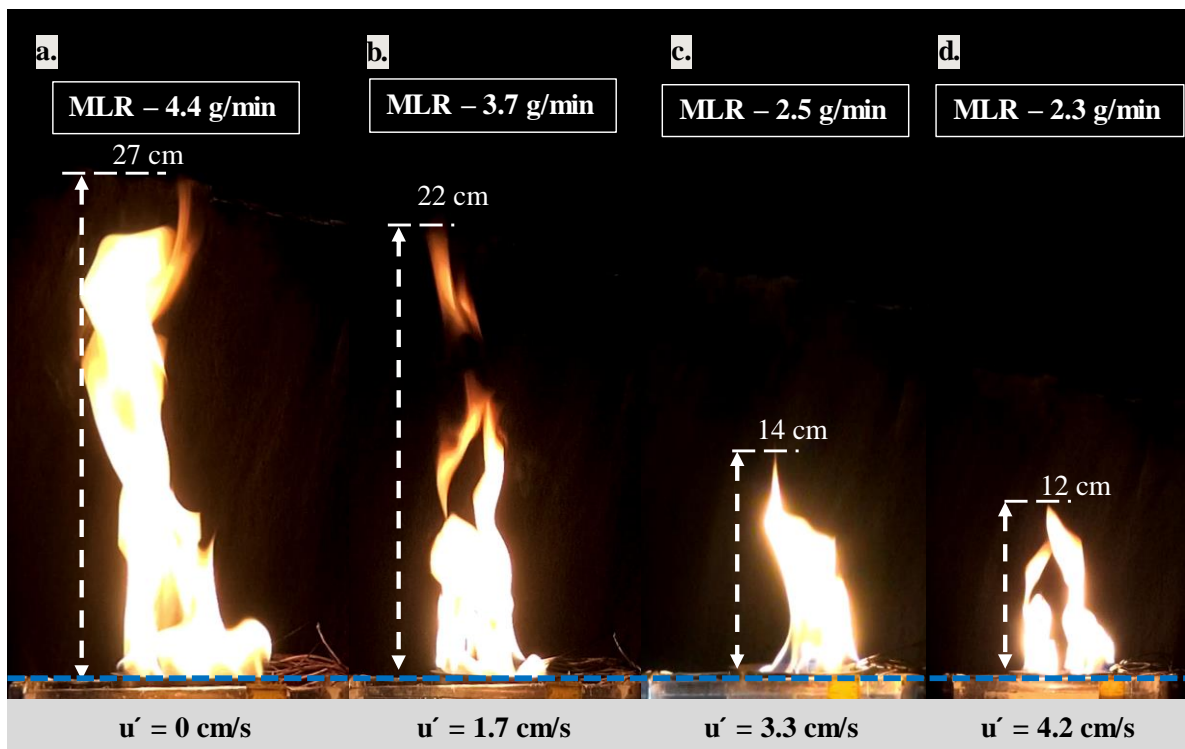


Figure 2.5. Photographs at 90 seconds into quasi-steady state burning of 5 mm n-dodecane fuel layer showing flame heights with increasing turbulence intensity. Cases showed at (a) $u' = 0$ (still water layer), (b) $u' = 1.7$ cm/s, (c) $u' = 3.3$ cm/s, and (d) $u' = 4.2$ cm/s.

It is noted that the wavy water sublayer causes a turbulent mixing effect and cools the fuel layer close to the water layer. The drastic effect of a wavy sublayer on the burning rate is thus shown in Figure 2.5 in terms of the burning rates and flame heights. To understand the mass burning rate trend as shown in

Figure 2.5., a heat transfer model has been developed using the temperature data. Figure 2.6., shows the schematic of the energy terms for the heat transfer used for analyzing the turbulence cases. For this study, the energy balance is considered at the interface of fuel and gas phase shown in red. The different heat input and loss terms (represented as \dot{q} in Watts) as shown in Figure 2.6., Subscripts (+) represents a heat input term, while (-) represents a heat loss term with respect to the fuel surface. Using these notations, $\dot{q}_{s(+)}$ is the conductive heat input at the fuel surface from the flame, $\dot{q}_{r(+)}$ is the radiative heat absorbed by the fuel surface from the flame, and $\dot{q}_{s(-)}$ is the heat transfer from the fuel surface to the in-depth of the fuel.

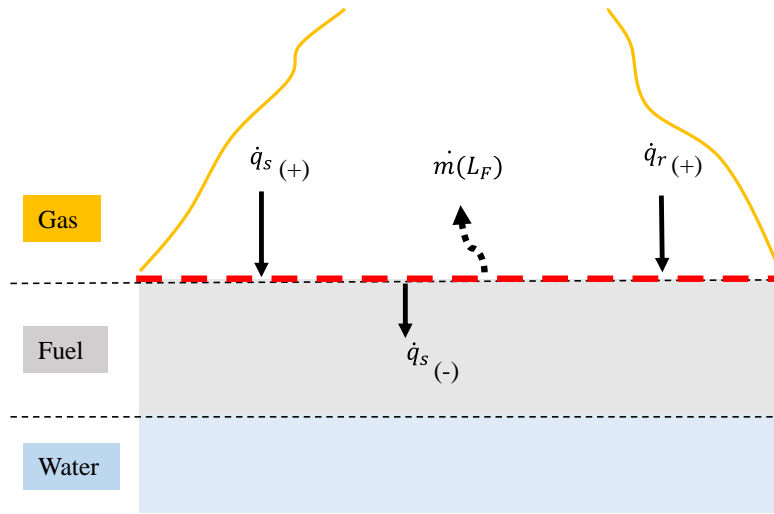


Figure 2.6. Fuel-air interface showing energy terms used for heat transfer model analysis.

For heat transfer analysis, the energy terms are expressed in the form of temperature gradient [48]. Conduction from the glass containment cylinder walls to the fuel surface is considered to be negligible as the glass cylinder is surrounded by a constant cooling bath. Hence, for this study, the term is not considered for overall energy balance.

$$\dot{m}(L_F) = \dot{q}_{r(+)} + \dot{q}_{s(+)} - \dot{q}_{s(-)} \quad (2.1)$$

In equation (2.1), $\dot{q}_{s(+)}$ is the energy input from the gas phase to the fuel surface, evaluated using thermocouple data in the gas phase and is given as shown in equation (2.2).

$$\dot{q}_{s(+)} = A_F k_{air} \left(\frac{dT}{dy} \right)_{y=0+}, \quad (2.2)$$

where, $y = 0$ represents the fuel-air interface, A_F is the fuel surface area, given as $A_F = A_{pool} = \pi \left(\frac{D^2}{4}\right)$, where D is the diameter of the pool. In equation (2.2), due to the reactions happening close to the fuel surface, the vapor space above the fuel can be considered as a gaseous mixture with nitrogen in abundance, hence k_{air} is used as the thermal conductivity of the air at an average gas phase temperature. $\left(\frac{dT}{dy}\right)_{y=0+}$ represents the temperature gradient at the gas/fuel interface considering the gas phase temperatures. It should be noted that the temperature gradient is obtained using a polynomial fit to the temperature measurements in the different phases. In equation (2.1), $\dot{q}_{s(-)}$ is given as

$$\dot{q}_{s(-)} = A_F k_{fuel} \left(\frac{dT}{dy}\right)_{y=0-}, \quad (2.3)$$

where, $\left(\frac{dT}{dy}\right)_{y=0-}$ represents the temperature gradient at the gas/fuel interface considering the fuel temperatures. k_{fuel} is used as the thermal conductivity of the dodecane fuel at an average liquid temperature.

In all cases tested, $\dot{q}_{r(+)}$ is the radiative heat absorbed by the fuel surface given by,

$$\dot{q}_{r(+)} = A_F \varepsilon \sigma (T_g^4 - T_s^4), \quad (2.4)$$

where ε is the emissivity considered to be 0.7 in this study [49], σ is Stephan Boltzmann constant ($5.67 \times 10^{-8} \text{ W/m}^2\text{K}^4$), T_g is the average temperature just above the fuel surface in the gas phase (K), and T_s is the surface temperature considered to be the saturation temperature of dodecane in Kelvin (489 K).

Using equations (2.1) – (2.4) above, the energy input $\dot{q}_{s(+)}$ from the flame and the net energy available for evaporating the fuel is plotted as a function of increasing turbulence intensity in Figure 2.7. The energy values are averaged across the three trials in the quasi-steady state region for each of the cases and the error bars show the uncertainty across these trials.

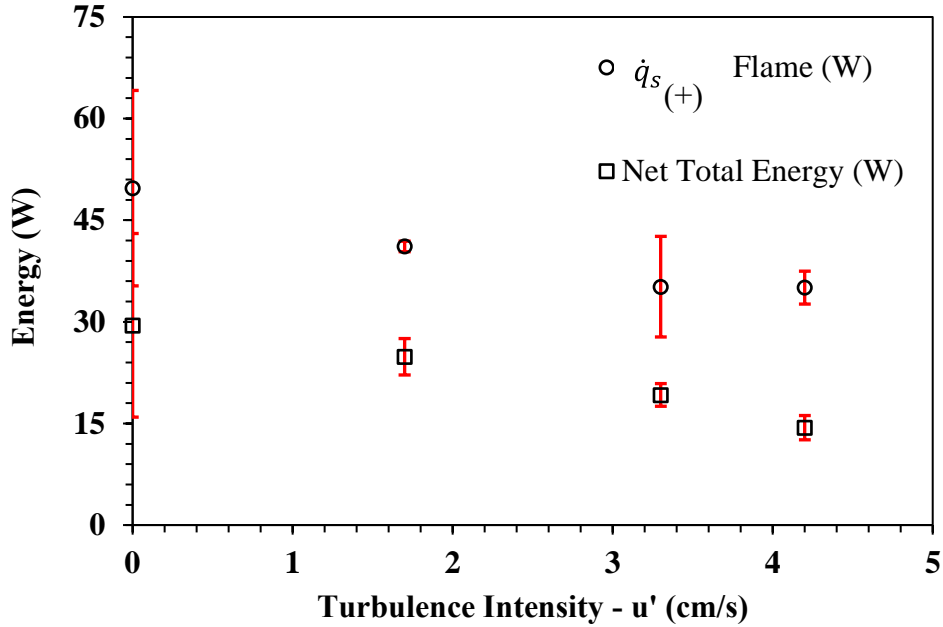


Figure 2.7. Energy input from the flame [$\dot{q}_{s(+)}$], and net total energy available for fuel vaporization [$\dot{m}L_F$] terms obtained using thermocouple data for n-dodecane fuel burning as a function of turbulent intensity (u').

The energy available from the flame considering the gas phase temperature gradient progressively declines with an increase in turbulence intensity. The decrease in energy from the flame reduces from 47.4 W for a baseline – no turbulence case to 35.07 W for the highest turbulence case at $u' = 4.2$ cm/s. Similarly, the net total energy available by the fuel [$\dot{m}(L_F)$] also decline from 27.1 W to 24.9 W, 19.2 W, and 14.4 W at $u' = 0, 1.7, 3.3,$ and 4.2 cm/s respectively, showing a 47% reduction in the energy values from the baseline to highest turbulence case tested.

Figure 2.8., shows the calculated mass burning rate across 4 cases ($u' = 0, 1.7, 3.3,$ and 4.2 cm/s turbulent intensity), using the energy balance as described and compared to the experimental burning rate obtained from the fuel replenishing system. The obtained burn rate values are plotted as a function of the turbulent intensity (u') of water. The red lines indicate a deviation error across 3 trials for every case. It is seen that the calculated values using the heat transfer model are in good agreement with the experimental

values and fall within the error margin of 20%, showing the energy balance and quantification of the heat input terms and heat loss terms are reliable and accurate.

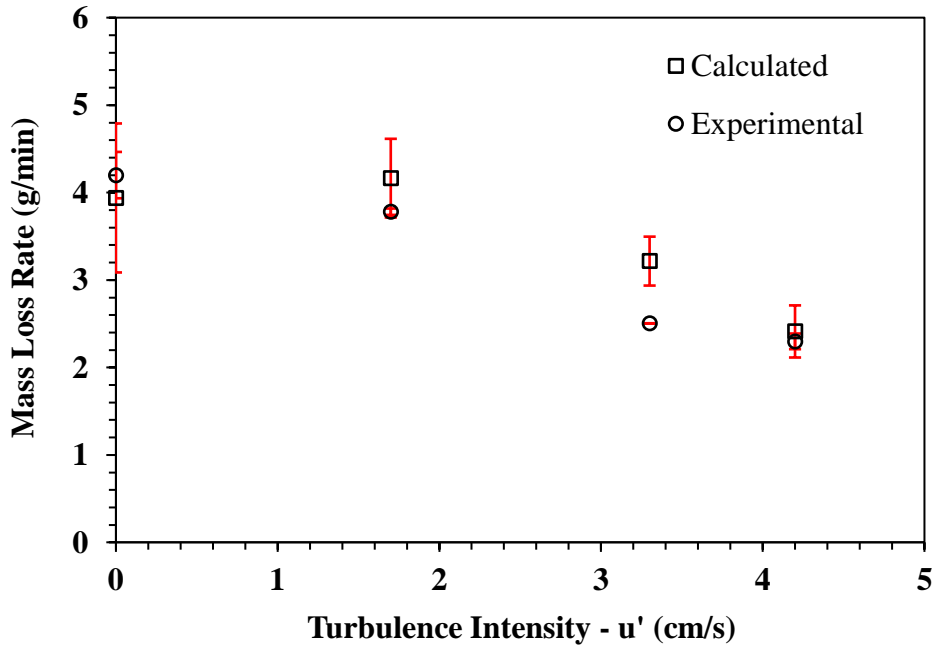


Figure 2.8. Calculated burning rate from the heat transfer model in comparison to the experimental burning rate obtained directly from the fuel replenishing system for baseline and three turbulent intensities (u').

2.4.2. *Transient Burn*

The quantification of heat transfer coefficient is key in realizing the effect of the turbulence.

Generally, this is evaluated using the heat loss at fuel-water interface defined as $\dot{q}_{loss,w} = A_F k_w \left(\frac{dT}{dy} \right)_{f-w}$.

Due to the wavy water sublayer, it was seen that the evaluation of the temperature gradient at fuel water interface was not accurate. As a result, a different approach is proposed here by analyzing the fuel temperature data during the transient stage of the burn (as shown in Figure 2.4). Three timestamps were chosen to analyze the temperature evolution with regressing fuel and its interaction with the surrounding water sublayer. 100 s, 250 s, and 400 s represent the timestamp from which the continuous fuel feeding system was stopped. Thus, the temperature obtained is said to be from the transient region. Figure 2.9 shows

the comparison of in-depth temperature data for two extreme cases (no turbulence and highest turbulence) from the fuel surface. The temperatures in the liquid fuel until extinction are shown. Zhao et al. [51] in his studies from kerosene pool fires observed an increase in liquid temperature with regressing fuel where the water sublayer under it was stagnant. Additionally, as time progressed Ito et al. and Inamura et al. [22-23] observed the temperature gets hotter in the fuel. The current study also observes a similar trend in the absence of any turbulent behavior ($u' = 0$ cm/s), where a reduction in the fuel thickness increases the overall heating in the fuel layers. This is clearly seen in Figure 2.9 (a) where the temperature increases from 100 s to 250 s. For a turbulence case ($u' = 4.2$ cm/s), the overall temperature is lower compared to the baseline case. In the case of turbulence, the temperature in the fuel keeps reducing from 100 s and 250 s. This is different from previous studies with still water where a temperature increase was observed. It is noteworthy, in both cases the temperature increases towards the extinction of flames at 400 s as the fuel regresses.

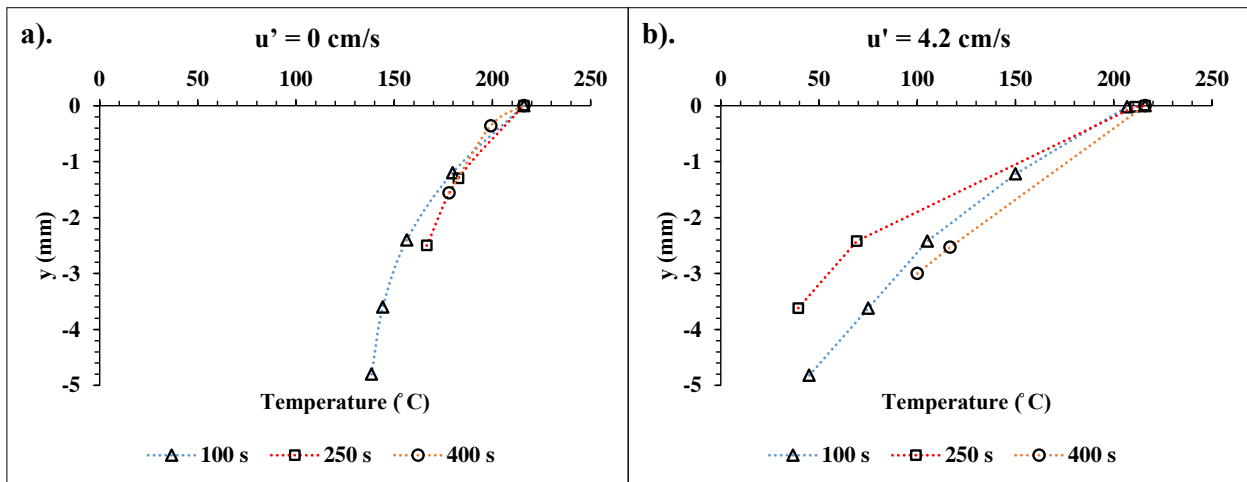


Figure 2.9. In-depth temperature in the fuel vs. relative position of the thermocouples comparing a). baseline – no turbulence case and b). worst- turbulence case ($u' = 4.2$ cm/s).

In summary, convective cooling from turbulence tends to cool the fuel layer. This also prolongs the burn as additional heat is required for fuel heating. Thus, the flames extinguish gradually, and the efficiencies reduce significantly in the presence of turbulence.

Quantifying the value of the heat transfer coefficient that leads to heat loss at the fuel-water interface is important based on the trend observed in Figure 2.9. To determine this coefficient value, a 1D heat conduction equation is considered for the fuel layer as shown in equation (2.5).

$$\frac{\partial T}{\partial t} = \alpha \frac{\partial^2 T}{\partial y^2} \quad (2.5)$$

where T is the temperature along depth y of the fuel and α is the thermal diffusivity of the fuel. At a particular timestep t when the fuel thickness is δ , we can say that, The fuel surface ($y = 0$) can be assumed to be at the saturation temperature of the fuel ($T_b = 216$ °C). At the fuel-water interface ($y = \delta$),

$$-k \left. \frac{dT}{dy} \right|_{y=\delta} = h(T_\delta - T_\infty) \quad (2.6)$$

In equation (2.6), k is the thermal conductivity of the fuel, h is the heat transfer coefficient as driven by the turbulence intensity of the water sublayer, T_δ is the fuel-water interface temperature, and T_∞ is the ambient water temperature. Assuming a linear temperature gradient in the thin fuel layer, the fuel-water interface temperature (T_δ) can be evaluated as,

$$T_\delta = \frac{T_b + \frac{h\delta}{k} T_\infty}{\left(1 + \frac{h\delta}{k}\right)} \quad (2.7)$$

Hence, T_δ is a function of δ which is a function of time. It is key to note that T_δ is a function of heat transfer coefficient h , which is again a function of the turbulence intensity. Thus, equation (2.7) has been identified as the “h-model” in this study as it is used for quantifying the coefficient. The value of ‘ h ’ is evaluated using an iterative method, such that the value T_δ at different time steps match the experimentally measured temperature value with minimum error. The error summation over the time between the experimental and calculated values is given as,

$$\varepsilon = \sqrt{\sum_t [T_\delta(\text{Experiment}) - T_\delta(\text{h-model})]^2} = \sqrt{\sum_t \left[T_\delta(\text{Experiment}) - \frac{T_b + \frac{h\delta}{k} T_\infty}{\left(1 + \frac{h\delta}{k}\right)} \right]^2} \quad (2.8)$$

The error ε in equation (2.8) is minimized by changing the value of h . The ambient water temperature is 20° C. The predicted fuel-water interface temperature (T_δ) is plotted in Figure 2.10 as a function of time for h values obtained from the minimum error analysis for one test per case of turbulence. The experimental values for T_δ at different time steps are also plotted for comparison with the predicted data. The value of the heat transfer coefficient as a function of turbulence is shown in Figure 2.11.

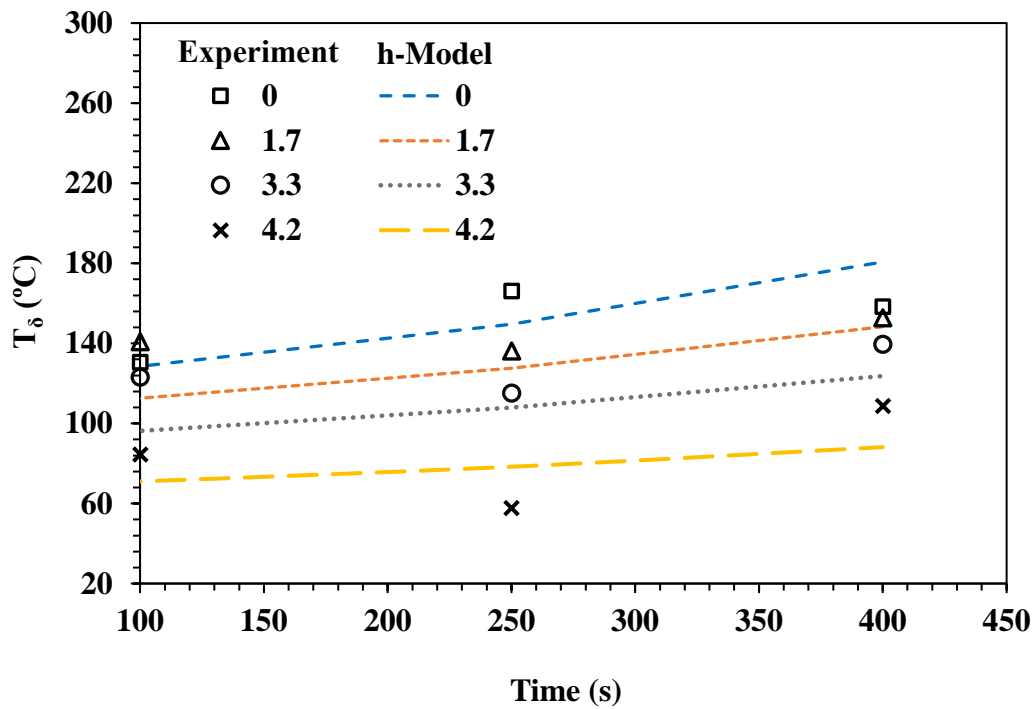


Figure 2.10. Comparison of the predicted and experimental values for fuel-water interface temperature (T_δ) as a function of time

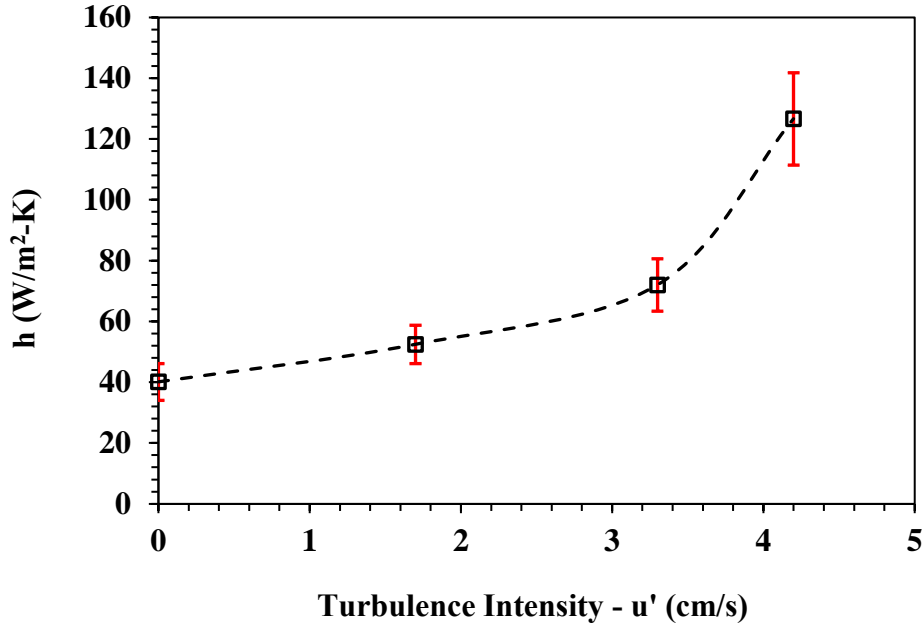


Figure 2.11. Calculated heat transfer coefficient values as a function of turbulence intensity (Baseline - $u' = 0$ cm/s $u' = 1.7$ cm/s, $u' = 3.3$ cm/s, $u' = 4.2$ cm/s). The value of h is obtained by minimum error analysis.

The values as shown in Figure 2.11 represent the best value for h for minimum error ε for each of the turbulence cases. The error bars show the variation in the value based on the three repeat trials. It is seen that the heat transfer coefficient increases from about 40 W/m²-K to about 125 W/m²-K with varying turbulence. This shows that as the turbulence increases, the cooling effect of the water sublayer is enhanced. This is further shown in Fig. 2.10, where the temperature at the fuel-water interface is seen to be much lower as the turbulence intensity increases. This subsequently reduces the burning rates at higher turbulence.

2.5. Conclusion

Experiments were performed to understand the heat transfer boundary condition at the fuel-water interface when introduced to turbulent wavy water. Turbulence was created using a submerged jet pointing upwards that created an isotropic region for testing. Results from the experiments showed turbulence has a significant effect on the burning behavior of fuel. The burning rate declined by 44% from 0.53 mm/min to

0.29 mm/min as the turbulence intensity increased from 0 cm/s (no turbulence) to 4.2 cm/s. The flame height also showed a reduction from 26 cm to 12 cm from no turbulence case to the highest case tested at $u' = 4.2$ cm/s, respectively. The energy balance at the fuel-air interface shows that the net energy for fuel to vaporize and burn reduces with increase in turbulence. A model was developed to determine a heat transfer coefficient as a function of the turbulence intensity. The model predicted that the convective heat transfer coefficient increased from 40 W/m²-K to about 125 W/m²-K for increasing turbulence intensity. Thus, the convective cooling increased significantly in the presence of surface turbulence below the fuel slick. Thus, the study gives insight into the effect of the turbulent water layer on the burning of thin fuel slicks as applicable to in-situ burning.

Chapter 3: Influence of Immersed Conductive Objects on Quasi-Steady Burning Behavior of Fuel Slick in Turbulent Waters

3.1. Preface

The reduction in the burning rate due to turbulence has been analyzed in Chapter 2. As a countermeasure to this reduction, during ISB, immersed conductive objects are placed to enhance the burning of oil slick on wavy water. The effect of these immersed objects in the presence of a quantified turbulent field is analyzed in this chapter. Further, the optimal immersion depth of this object is proposed towards advancing the use of these objects for the in-situ burning technique.

3.2. Experimental Methodology

Figures 3.1 and 3.2 show the experimental platform for studying fuel burning on wavy water with an immersed copper rod. The experimental platform is similar to the one used in Chapter 2, where a 100 mm circular containment sits inside a 200 mm x 200 mm larger containment. The setup uses a fuel-feeding system using a syringe pump. Experiments are performed using n-dodecane due to its similar boiling point and well-defined thermo-physical properties of this single-component fuel.

A 10 mm diameter copper rod as shown in Figures 3.1 and 3.2 is used as an immersed conductive object. For ISB operations the oil contained at the back of the boom can range from 5 mm to 170 mm depending on the oil spill volume, the towing speed, and the boom draft [53]. In this study, a 40 mm fuel slick is considered with the immersed rod. This is the maximum fuel thickness that can be tested in the current setup considering the confined isotropic region. In the analysis, the effect of the immersed depth of the rod in the fuel is studied by placing the rod at depths 5 mm, 10 mm, 20 mm, 30 mm, and 50 mm from the fuel surface. The ullage is maintained at 10 mm across all tests for this study. The immersed portion of the rod (heater region) distributes the heat to the fuel thus preheating and vaporizing the fuel. It is noted that for these different immersion depths, the top portion (collector) of the copper rod is always exposed to the flames (collector region) that heat up during the burn. As the focus of the study is to determine the optimum heater configuration, the length of the copper rod in the flame is always maintained at 140 mm

across all immersion depths analyzed in the study. The total length of the rods is thus different for different immersion depths.

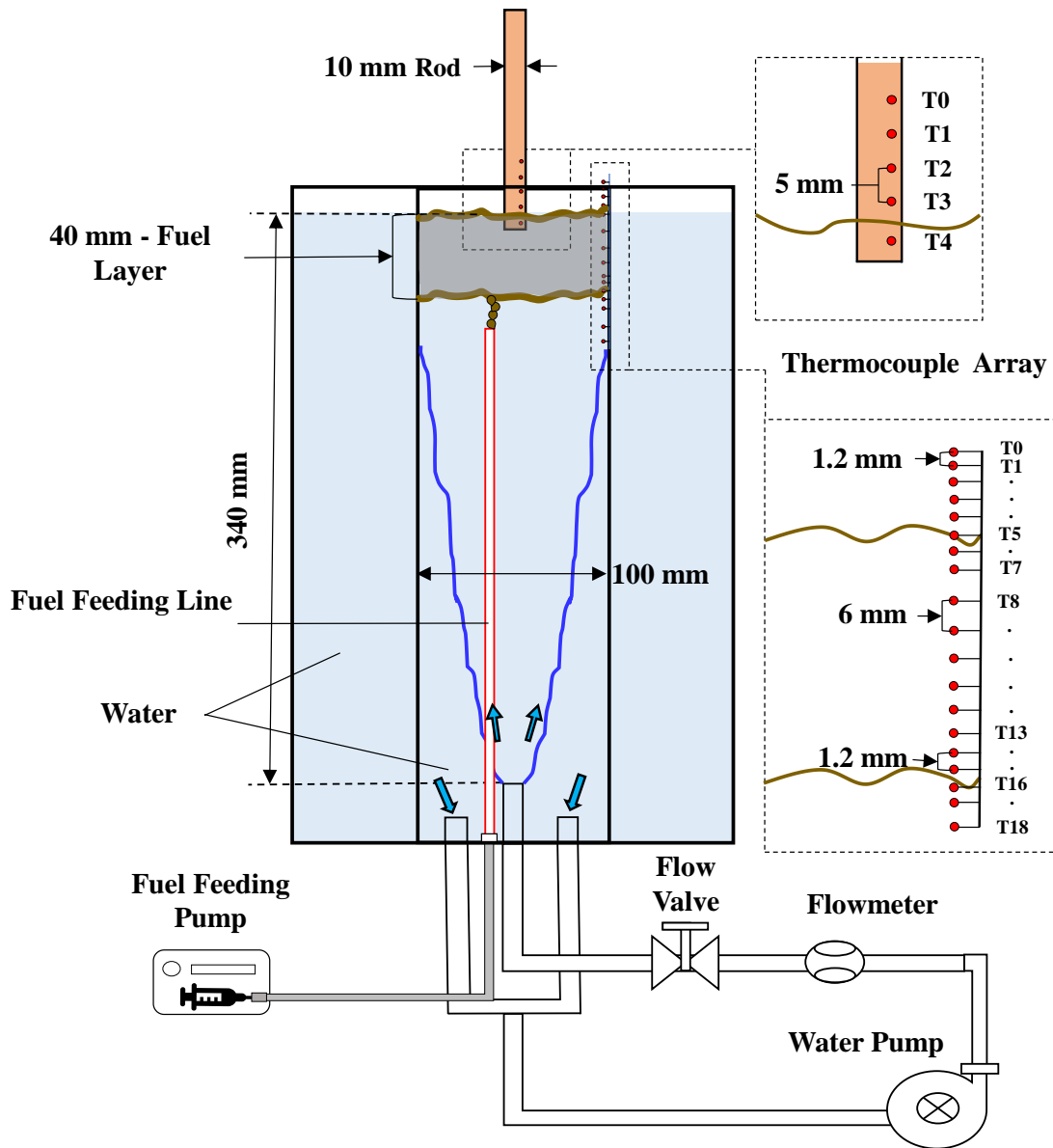


Figure 3.1. Schematic diagram of the experimental platform for fuel burning on wavy water with continuous fuel feeding setup and an immersed rod; inset images show thermocouple locations on the rod surface; and in gas, fuel, and water phases.

Experiments were carried out from $u' = 0$ cm/s to $u' = 3.3$ cm/s in Chapter 2 for understanding influence of turbulence in detail. For this study, an intermediate turbulent intensity of $u' = 1.7$ cm/s is chosen

to analyze the effect of immersion depth on the burning behavior of the liquid and consequently analyze the boundary conditions associated with it. The observed maximum vertical fluctuations in the fuel from the turbulence experiments were higher for 3.3 cm/s and 4.2 cm/s cases, affecting the fuel-water interface monitoring. Hence, for this study, the tests were conducted at an intermediate turbulent intensity of $u' = 1.7$ cm/s across all tests.

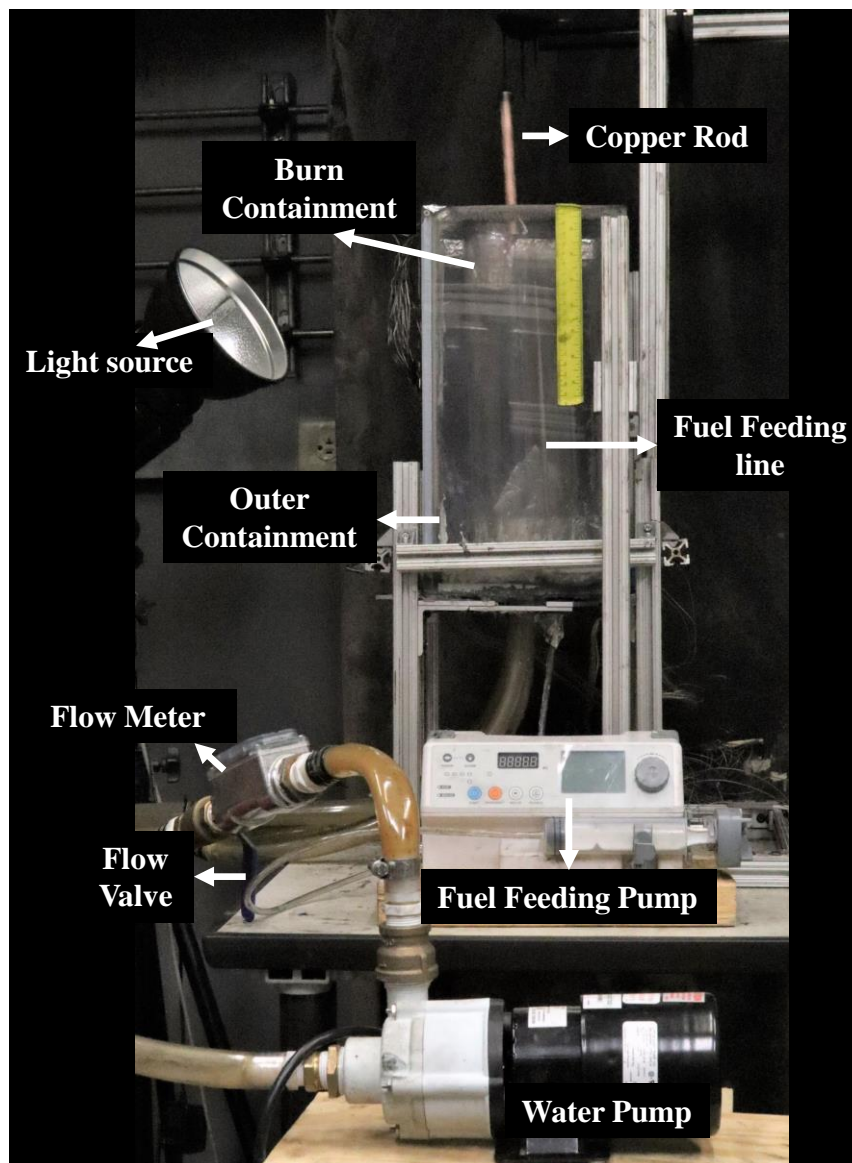


Figure 3.2. Experimental platform for fuel burning on wavy water with continuous fuel feeding setup and an immersed rod.

Figure 3.1 also shows a vertical array consisting of 19 Omega K-type 36-Gauge thermocouples that have been placed in the inner cylinder to measure water, fuel, and gas phase temperatures. Thermocouples near the interfaces are placed 1.2 mm apart to ensure refined measurements and accurate evaluation of the temperature gradients at the gas-fuel and fuel-water interfaces. The thermocouples in the bulk fuel region are placed 6 mm apart to measure the overall gradient in fuel temperature. The total span of the thermocouple in the three phases is 63.6 mm. The copper rod surface is also embedded with thermocouples at 5 mm spacing as shown in Figure 3.1., to analyze the overall heat transfer from the rod to the liquid layers. Data from the thermocouples are sampled at a frequency of 1 Hz for all experiments.

The outer chamber is filled with water and the pump is initiated with a set flow rate equivalent to the turbulent intensity of $u' = 1.7$ cm/s. The setup is allowed to run idle for 10 minutes to stabilize the flow to the inner tube and eliminate any trapped air in the flow tube. Once the set flow is achieved, fuel is introduced from the top, corresponding to a 40 mm layer by weight (236.3 g) using the measured density of liquid n-dodecane which is 752.2 kg/m³. A propylene torch is used to ignite the fuel that is contained in the cylindrical tube. The fuel feeding is initiated from the syringe pump 10 seconds from the ignition. A fuel thickness of 40 mm is maintained by adjusting the feeding rate of the pump using level markings on the glass tube.

Additionally, a loadcell is used to record the overall mass of the setup as a secondary validation. Figure 3.3., shows the mass loss rate of the overall system observed from the scale placed under the setup as backup monitoring system. The burning rate observed at a steady state from the feeding pump is considered as the mass burning rate for the test.

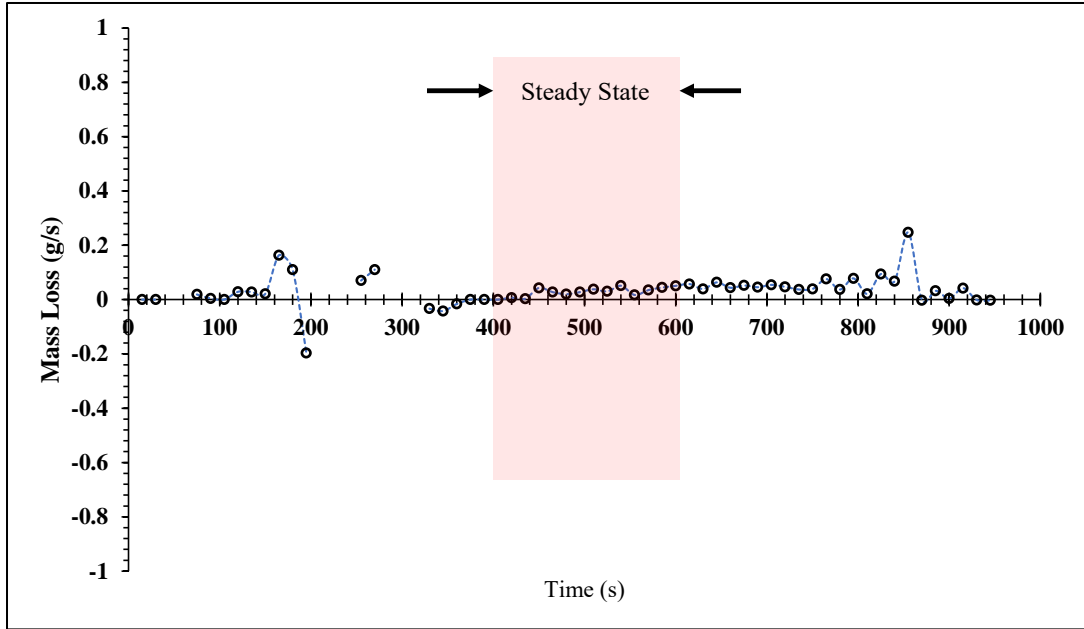


Figure 3.3 Mass loss rate plotted against time to show progression of burning across the experiment for baseline case.

The deviation in the mass loss rate is reported as the standard deviation from the average flow rate value across 3 trials for each case. The uncertainty observed in monitoring the fuel thickness of 40 mm is ± 0.1 mm across the defined steady state, as measured by post-processing the fuel-water interface images as shown in Figure 3.4. Flame heights for the time stamps shown are measured using an open-source software ‘ImageJ’. A reference length is known by using a measuring scale in the image. This reference length scale is converted into pixel scale to obtain pixels/cm. This Pixel-length relationship is then used to obtain the visible flame heights in the figure. The flames are measured from the rim of the containment setup to the tip of the continuous flame for the figures shown in the subsequent sections.

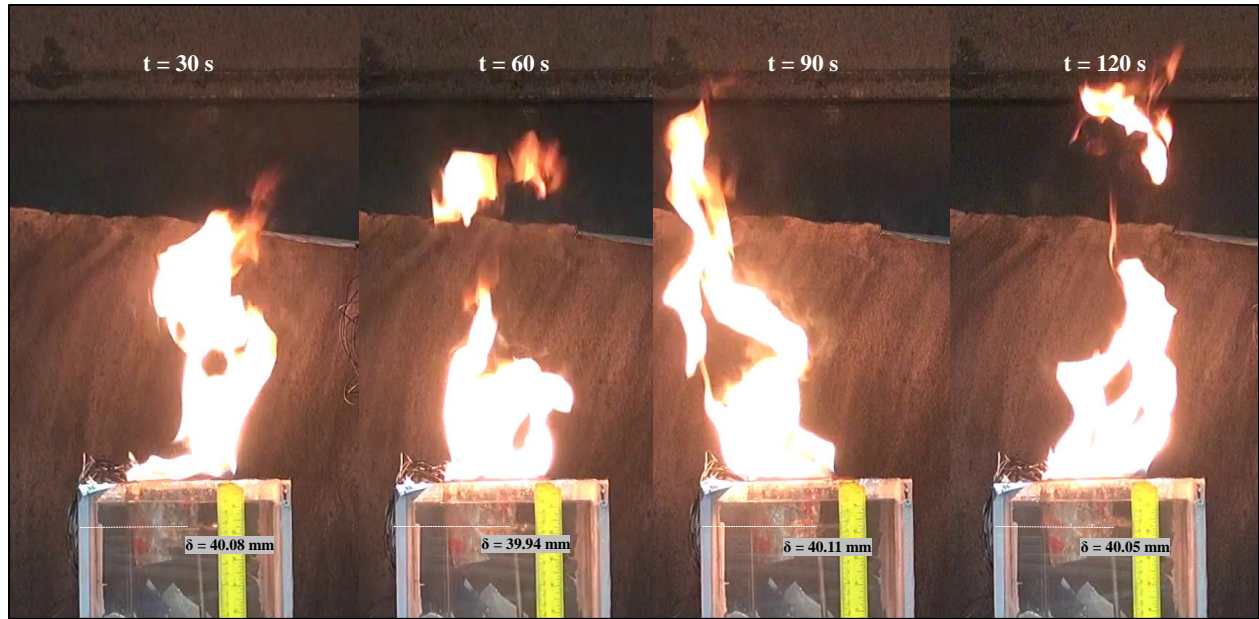


Figure 3.4. Images of baseline case with fuel level marked and measured at 30, 60, 90, and 120 seconds into achieving quasi-steady state.

3.3. Results and Discussion

3.3.1. Effect of Rod Depth

Different immersion depths are considered to understand the effect of rod depth on the heat transfer and burning characteristics of the fire. The five depths considered are 5 mm, 10 mm, 20 mm, 30 mm, and 50 mm for preliminary analysis. As the fuel is 40 mm, these depths correspond to cases where (a) the rod is immersed in only fuel layer: 5 mm, 10 mm, 20 mm, and 30 mm, and (b) the rod is immersed in fuel and water layers: 50 mm. In all the cases, the section of the rod exposed to flame (collector region) has a height of 140 mm consistently such that only the copper rod immersed in the liquid phases (heater region) is varied. Additionally, a baseline case with no rod is also carried out for comparison.

Figure 3.5 shows the results for the mass burning rate. The mass loss rate is evaluated as the feeding rate from the fuel replenishing pump required to maintain the constant 40 mm fuel thickness. The overall mass loss rate is plotted against their corresponding rod depth in Figure 3.5. The baseline case with no rod in the system has a mass burning rate of 3.75 g/min and is compared against rod cases at various depths. A mass burning rate of 5.5 g/min is the maximum observed burning rate for cases considered. This maximum

burning rate corresponds to the case where the copper rod is immersed at 5 mm and 10 mm. At rod depths of 20 mm and 30 mm in the fuel, the burning rate reduced to 4.21 g/min and 4.22 g/min, respectively. At 50 mm depth, where the rod is both in the fuel layer and water sublayer, the mass burning rate is lowest among the immersed cases at 4.14 g/min. These results show that the burning enhancement reduces with the proximity of the rod to the wavy water sublayer. Thus, immersion depth of the rod is a key parameter in achieving optimal burning rates in the presence of the immersed rod. Further analysis is thus done in this study to quantify the effect of the rod depth on the heating mechanism of the fuel and to understand the subsequent burning behavior.

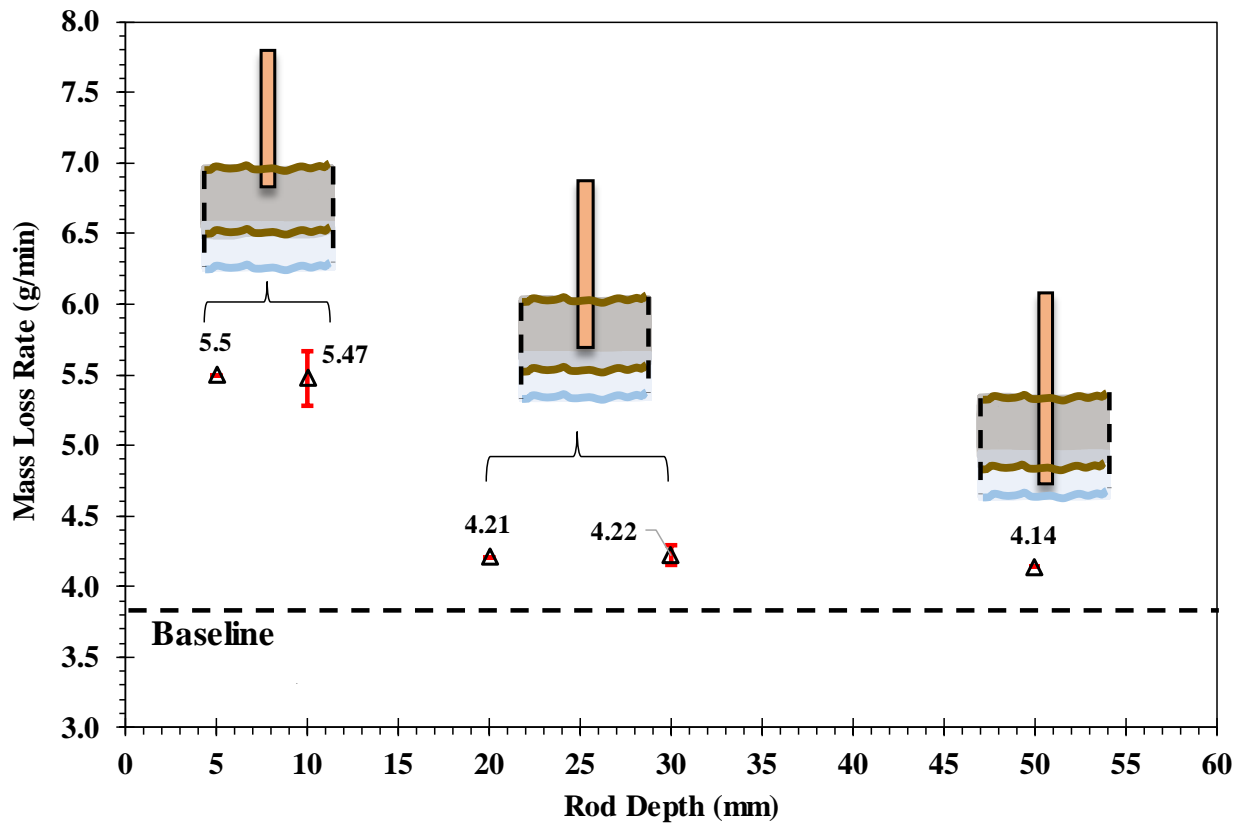


Figure 3.5. Mass loss rate of the burning fuel as a function of rod depth for 5 mm, 10 mm (rod immersed close to fuel surface), 20 mm, 30 mm (rod partially immersed in fuel), and 50 mm (rod immersed in fuel and water). Error bars presented with a standard deviation of three repeated experiments.

Figure 3.6 (a) - (c) shows the flame photographs when the copper rod is immersed at depths 10 mm, 30 mm, and 50 mm from the fuel surface at 90 seconds of achieving a quasi-steady state. A baseline case is also shown to compare the test matrix for comparison. The highest flame height is seen with a copper rod immersed at 10 mm from the fuel surface with flames reaching up to 47 cm high. The flame height is seen to reduce when the rod is placed closer to the water sublayer at 30 mm and 50 mm from the fuel surface. The corresponding flame height is observed to be 40 cm and 37 cm for the two cases as shown in Figure 3.6. This shows that the wavy water sublayer acts as a heat sink, cooling the lower section of the fuel layer and the immersed rod. The baseline case (no rod) shows the lowest flame height and least burning rate compared to the rod cases, with a flame height of 23 cm.

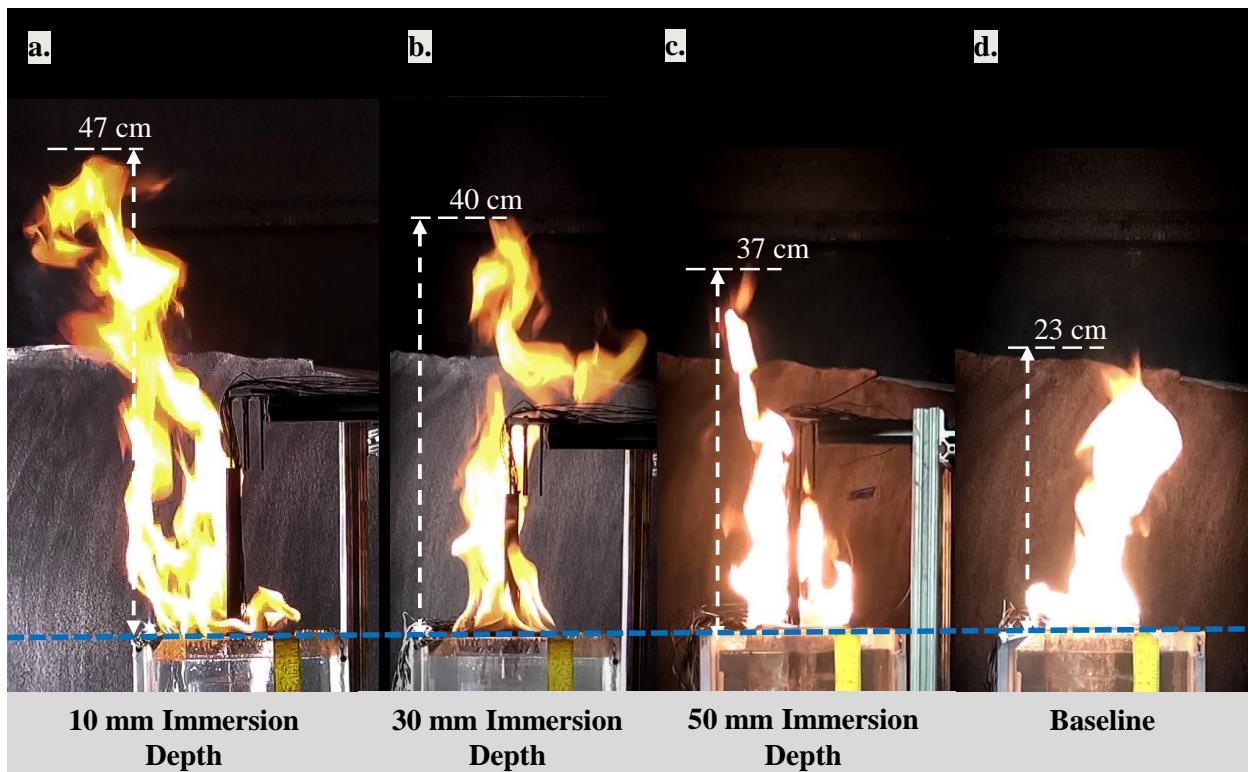


Figure 3.6. Photographs at 90 seconds into quasi-steady state burning of 40 mm n-dodecane fuel layer showing flame heights at the turbulence of $u' = 1.7$ cm/s. Cases showed at rod depths: (a) 10 mm, (b) 30 mm, (c) 50 mm, and (d) baseline (no rod).

The definition of a quasi-steady state by fuel replenishment is described here. Figure 3.7 shows the time evolution of an experiment with a rod immersed at a depth of 50 mm from the fuel surface under the influence of $u' = 1.7$ cm/s. The thermocouples sampled at 1 data point/second (1 Hz) are averaged at 15-second intervals to smoothen and reduce the noise in the data.

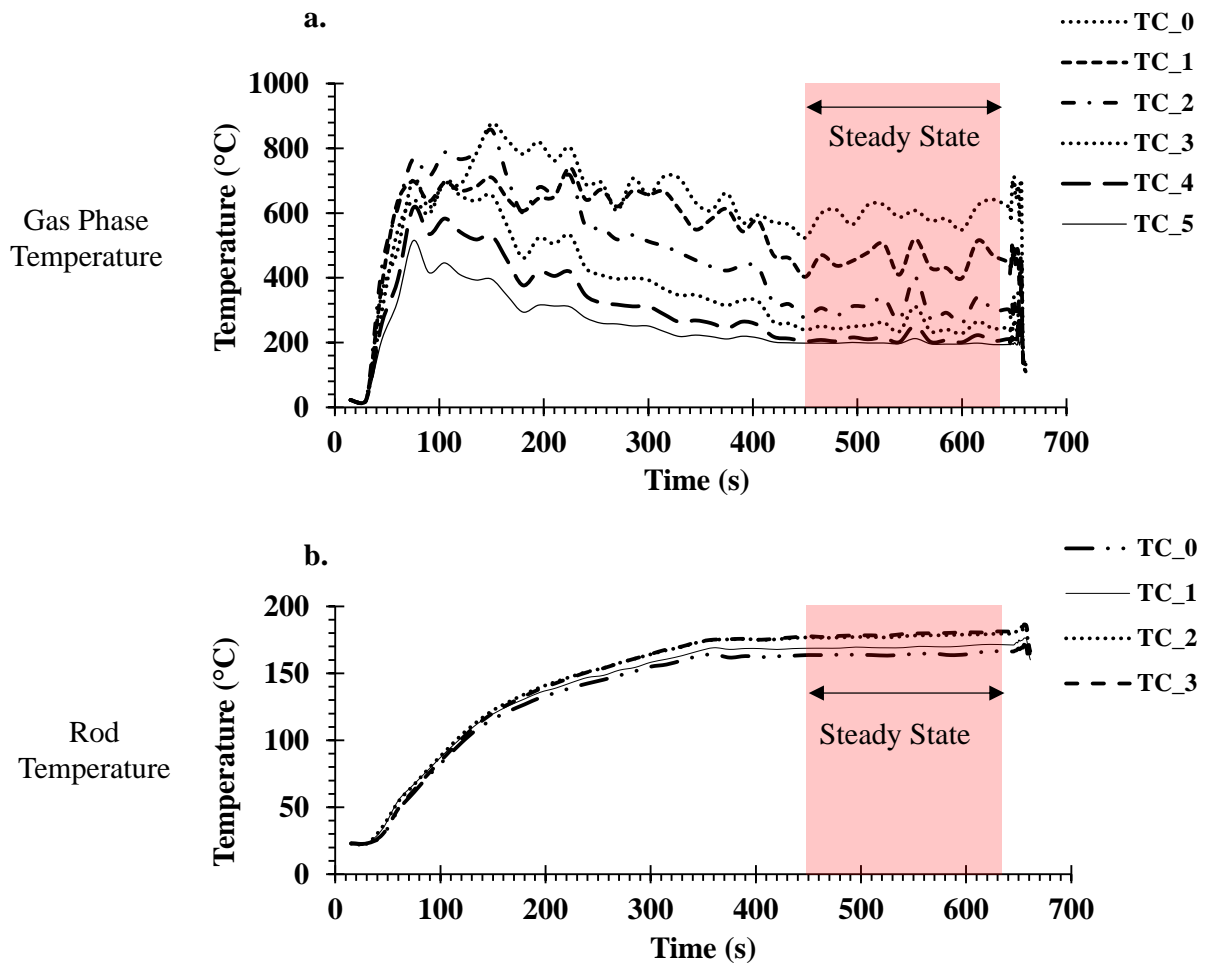


Figure 3.7. Time evolution of 50 mm rod experiment at turbulent intensity $u' = 1.7$ cm/s marked with a defined steady-state region. (a) shows temperatures in the gas phase, and (b) shows temperatures in the rod.

The experiment begins with ignition at $t = 30$ s. The fuel is fed continuously from $t = 40$ s and feeding is stopped at $t = 645$ s. The fire is quenched manually at $t = 650$ s as shown in Figure 3.7. The temperatures in the gas phase and on the rod surface until extinction are shown. The fuel level is maintained

at 40 mm across the duration of the experiment. Steckler et al [52] reported that the oil and water sublayer after ignition endure a transient heat process after which the temperatures stabilize and fuel regresses at a steady rate. For the current study with fuel replenishment, “*when the variation in the temperature gradient in the gas phase and the rod is less than 10% and 5% respectively, the system is considered to be in a quasi-steady state*”.

Figure 3.7 (a). shows the region in red from $t = 450$ s to $t = 630$ s that represents the defined steady-state observed in the gas phase. Similarly, Figure 3.7 (b). shows the temperatures rising on the rod surface from $t = 30$ s to $t = 350$ s which is the heat-up period. From $t = 450$ s to $t = 630$ s, the temperatures attain a steady value which also corresponds to the gas phase temperature steady region shown in Figure 3.7 (a).

3.3.2. Heat Transfer Mechanism

To understand the mass burning rate trend as shown in Figure 3.8., an energy balance equation has been developed using temperature data. Figure 3.8 (a). shows the schematic of the energy terms for the heat transfer mechanism with the single copper rod immersed across the depth of the fuel and part of the rod immersed in the water layer. Figure 3.8 (b). shows the rod partially immersed in the fuel being exposed to the flame. The heat from the flame is collected by the rod surface in the gas phase. This heat is conducted through the liquid fuel layer. Thus, the fuel layer receives heat from the gas phase and additionally through the immersed copper rod. Figure 3.8 (c). shows the schematic for the baseline case without the presence of the copper rod.

In each case discussed, the control volume is defined as the dodecane fuel layer, with the different heat gain and loss terms (represented as \dot{q} in Watts) as shown in Figure 3.8. Subscripts (+) represents a heat input term, while (-) represents a heat loss term with respect to the control volume. Using these notations, $\dot{q}_s (+)$ is the conductive heat input at the fuel surface from the flame, $\dot{q}_{rod (+)}$ is the heat input from the copper rod cross-section area into the fuel, $\dot{q}_r (+)$ is the radiative heat absorbed by the fuel surface from the flame, $\dot{q}_{rod,loss (-)}$ is the heat loss at the rod surface in contact with the water layer, and $\dot{q}_{w,loss (-)}$ is heat loss from the fuel layer to the water layer.

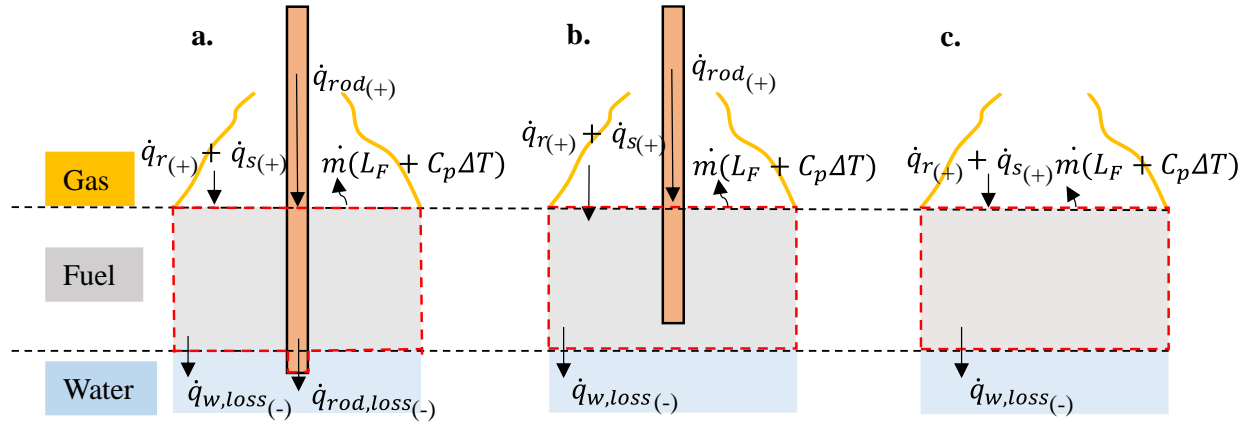


Figure 3.8. Control Volume (red dash Line) showing heat energy terms for the cases. (a) Copper rod immersed across the entire depth of fuel and partially in the water, (b) Copper rod immersed in fuel layer above the water sublayer, and (c) Baseline - no rod case.

For heat transfer analysis and modeling, all the energy terms are expressed in the form of gradient in temperature [48]. Conduction from the glass containment cylinder walls to the liquid pool is considered to be negligible as the glass cylinder is surrounded by a constant cooling bath. Hence, for this study, the term is not considered for overall energy balance.

Figure 3.8 (a) shows the energy balance for the immersed copper rod in fuel and water and given by,

$$\dot{m}(L_F + C_p\Delta T) = \dot{q}_{r(+)} + \dot{q}_{s(+)} + \dot{q}_{rod(+)} - \dot{q}_{rod,loss(-)} - \dot{q}_{w,loss(-)}, \quad (3.1)$$

where, L_F is the heat of vaporization of the fuel, C_p is the specific heat of the liquid fuel, and ΔT is the change in temperature during sensible heating. For the case where the rod is immersed only in the fuel, Fig. 3.7 (b) shows energy balance and the equation can be written as,

$$\dot{m}(L_F + C_p\Delta T) = \dot{q}_{r(+)} + \dot{q}_{s(+)} + \dot{q}_{rod(+)} - \dot{q}_{w,loss(-)}. \quad (3.2)$$

Figure 3.8 (c) shows the energy balance for the baseline which is the no-rod condition. For this case, the energy balance at the fuel surface can be written as,

$$\dot{m}(L_F + C_p \Delta T) = \dot{q}_{r(+)} + \dot{q}_{s(+)} - \dot{q}_{w,loss(-)}, \quad (3.3)$$

In equations (3.1) to (3.3), ΔT is defined as the temperature of the fuel during sensible and is given by, $(T_s - T_{avg})$, where, T_s is the surface temperature of the liquid pool as given by the saturation temperature of n-dodecane (216 °C). T_{avg} is the average fuel layer temperature in the quasi-steady burning period. It is noted that even with the fuel replenishment, T_{avg} is higher than the ambient inlet temperature as the bulk of the fuel is still at a higher temperature. Additionally, in-depth radiation absorption is not included in the model, and the average fuel temperature is accounted for the sensible heating.

In the three cases, $\dot{q}_{r(+)}$ is the radiative heat absorbed by the fuel surface given by,

$$\dot{q}_{r(+)} = A_F \varepsilon \sigma (T_g^4 - T_s^4), \quad (3.4)$$

where, A_F is the fuel surface area, given as $A_F = A_{pool} - A_{rod} = \pi \left(\frac{D^2}{4} - \frac{d_r^2}{4} \right)$ for cases with immersed rod and, $A_F = A_{pool} = \pi \left(\frac{D^2}{4} \right)$ for the case without the presence of a rod (baseline). And D and d_r are the diameter of the pool and the diameter of the rod respectively. ε is the emissivity is considered to be 0.7 in this study [49], σ is Stephan Boltzmann constant ($5.67 \times 10^{-8} \text{ W/m}^2\text{K}^4$), T_g is the average temperature just above the fuel surface in the gas phase (K), and T_s is the surface temperature of the liquid pool in Kelvin (489 K).

$\dot{q}_{s(+)}$ is defined as the energy input from the gas phase to the fuel surface, evaluated using thermocouple readings in the gas phase for all tests, and is given as shown in equation (3.5).

$$\dot{q}_{s(+)} = A_F k_{air} \left(\frac{dT}{dy} \right)_{y=0+}, \quad (3.5)$$

In equation (3.5), due to the reactions happening close to the fuel surface, the vapor space above the fuel can be considered as a gaseous mixture with nitrogen in abundance, hence k_{air} is used as the thermal conductivity of the air at an average gas phase temperature. $\left(\frac{dT}{dy} \right)_{y=0+}$ represents the temperature gradient at the gas/fuel interface considering the gas phase temperatures. It should be noted that the

temperature gradient is obtained using a polynomial fit to the temperature measurements in the different phases.

$\dot{q}_{w,loss(-)}$ is the heat lost from the fuel to the water layers and is defined using the temperature gradient at the fuel-water interface, and is given as,

$$\dot{q}_{w,loss(-)} = A_F k_{water} \left(\frac{dT}{dy} \right)_{fuel-w} . \quad (3.6)$$

For the rod, $\dot{q}_{rod(+)}$ is the heat conducted through the rod to the liquid layers is defined using the temperature gradient in the rod at the gas-fuel interface, and is given as,

$$\dot{q}_{rod(+)} = A_{rod} k_{rod} \left(\frac{dT}{dy} \right)_{rod-f} . \quad (3.7)$$

Similarly, $\dot{q}_{rod,loss(-)}$, is the heat loss to the water layer from the rod and is defined using the temperature gradient in the rod at the fuel-water interface and is given as,

$$\dot{q}_{rod,loss(-)} = A_{rod} k_{rod} \left(\frac{dT}{dy} \right)_{rod-w} . \quad (3.8)$$

Using the definitions and equations given above, the energy budgeting is shown in Figure 3.8 for the different cases. The terms represents the energy input terms [$\dot{q}_s(+)$, $\dot{q}_r(+)$, $\dot{q}_{rod(+)}$], energy loss terms [$\dot{q}_{rod,loss(-)}$, $\dot{q}_{w,loss(-)}$], and the net energy available for fuel heating and vaporization terms [$\dot{m}(L_F + C_p \Delta T)$]. The energy values are averaged across the three trials in the quasi-steady state region for each of the cases and the error bars show the uncertainty across these trials. The total energy input increases from the baseline case ($\dot{q}_s(+)$, $\dot{q}_r(+)$ = 54.2 W) to 10 mm rod depth and 30 mm rod depth case at ($\dot{q}_s(+)$, $\dot{q}_r(+)$, $\dot{q}_{rod(+)}$) = 68.4 W and 59.4 W, respectively.

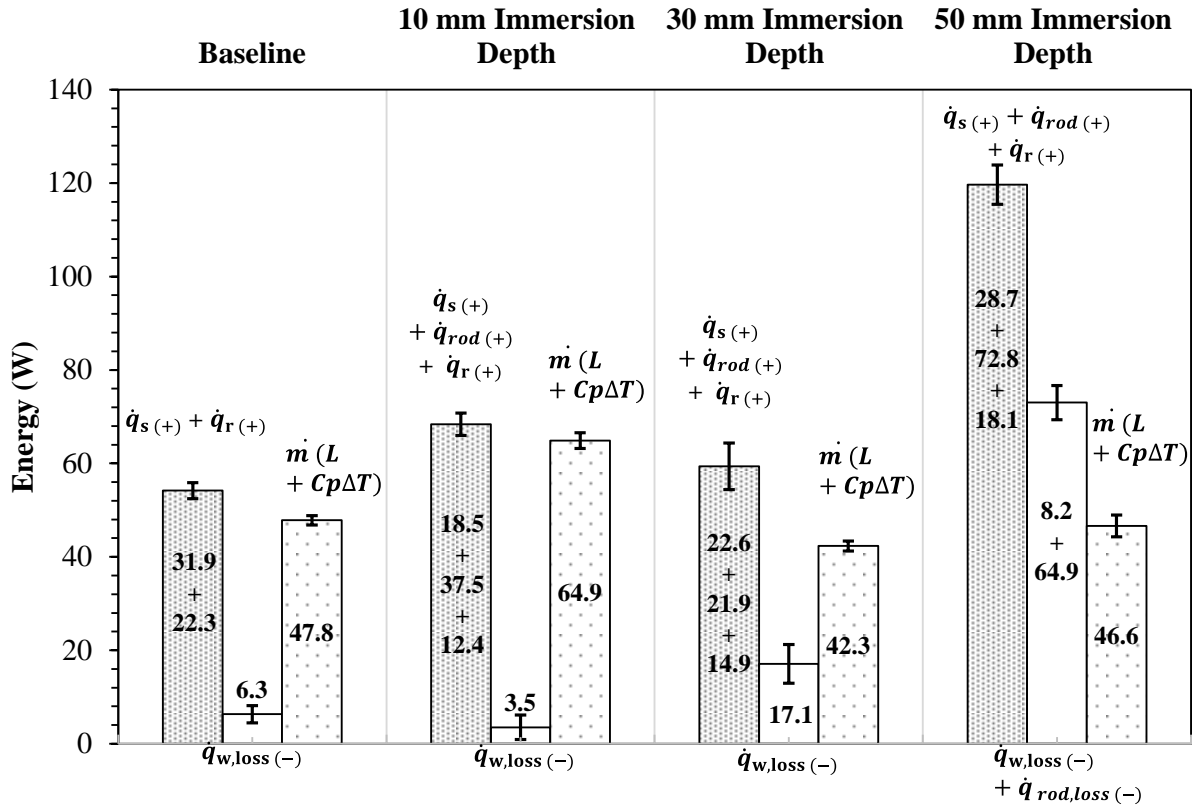


Figure 3.9. Energy budgeting chart showing the energy terms: energy input

$[\dot{q}_s(+), \dot{q}_r(+), \dot{q}_{rod}(+)]$, energy loss $[\dot{q}_{rod,loss}(-), \dot{q}_{w,loss}(-)]$, and overall energy available for fuel heating and vaporization $[\dot{m}(L_F + C_p\Delta T)]$; Obtained using thermocouple data for n-dodecane fuel burning under the turbulent intensity of $u' = 1.7$ cm/s.

The 50 mm rod depth shows significantly higher numbers, this is the result of the higher temperature gradient across the rod surface (with $\dot{q}_{rod}(+)$ being 72.8 W) as it is in contact with water. Also, $\dot{q}_s(+)$ + $\dot{q}_r(+)$ = 46.8 W for 50 mm rod depth case as an effect of the flames being shorter and closer to the fuel surface (low burning rate). Thus, the total energy input is 119.6 W. However, it is interesting to note that the energy available by the fuel $[\dot{m}(L_F + C_p\Delta T)]$ is almost similar with 30 mm and 50 mm immersion depths, despite the heat input being much higher for the 50 mm case. As the rod is immersed in water, the rod and fuel lose 73.1 W of heat to the water sublayer. Even though the energy input is high for the 50 mm case, a significant amount of the energy is lost to the water layer from the rod.

Thus, the energy budget indicates that the depth of the rod in the fuel layer plays an important role in the overall energy distribution required for enhancing the burning rate of the fuel. Figure 3.10 (a) shows this effect of rod depth on the energy loss to water [$\dot{q}_{w,loss(-)}$]. The losses are lowest for baseline and 10 mm case (< 10 W) as the fuel loses energy to wavy water. For the 30 mm immersion depth, it is seen that the in-depth layers of the fuel layer are heated further by the immersed rod and the heated fuel loses about 17.1 W of heat to the water sublayer, which is higher than the 10 mm case. For the 50 mm case, the loss is given by [$\dot{q}_{rod,loss(-)} + \dot{q}_{w,loss(-)}$] as the rod is immersed in water as well and the corresponding energy loss observed is 73 W.

For the copper rod immersed at 10 mm depth, $\dot{q}_r(+)$ + $\dot{q}_s(+)$ is about 30.8 W and $\dot{q}_{rod(+)}$ is 37.5 W, summing up to 68.4 W. The additional mass loss rate due to the rod can be evaluated as $\dot{m}_{rod} = \dot{q}_{rod(+)} / (L_F + C_p \Delta T)$. Figure 3.10 (b) shows this additional mass loss rate as a function of immersion depth. It is seen that \dot{m}_{rod} is highest for the 10 mm case and reduces as the immersion depth increases. This is because $\dot{q}_{rod(+)}$ reduces to about 22 W for a 30 mm case. The increase in the burning rate is the effect of the rod heating the fuel layer and vaporizing the fuel. To analyze this effect further, a thermal penetration depth is derived using the energy equation shown below,

$$\frac{\partial T}{\partial t} = \alpha \frac{\partial^2 T}{\partial y^2} \quad (3.9)$$

Performing an order of magnitude analysis, we get

$$\frac{\Delta T}{t} \sim \alpha \frac{\Delta T}{\delta^2} \rightarrow \delta \sim \sqrt{\alpha t} \quad (3.10)$$

In equation (3.10), δ is the thermal penetration depth, t is the time to reach a steady state from the ignition, α is the thermal diffusivity of the fuel given as, $\alpha = \left(\frac{k}{\rho C_p} \right)_{fuel}$; where, k is the thermal conductivity, C_p is the specific heat and ρ is the density of the fuel. Using the properties of n-dodecane, it is seen that thermal penetration depth (δ) is ~ 10 mm from the fuel surface. This upper depth of the fuel can thus be defined as a hot zone. For further analysis of the hot zone, Figure 3.11 shows the two cases with copper rods

immersed at 30 mm and 10 mm depth. Small bubbles are observed on the top 10 mm of the rod surface indicating significant nucleate boiling in the hot zone. As the immersion depth increases, the lower fuel layers are also heated by the rod with reduced energy available for nucleate boiling. Moreover, the higher bulk fuel temperature leads to higher heat loss to water to about 17.1 W in the 30 mm case as compared to 3.5 W for the 10 mm rod depth case (Figure 3.9 and Figure 3.10 (a)). Thus, it can be justified that rod depth within the hot zone is an optimal condition for enhanced burning. Additionally, it is to be noted that for 50 mm depth, $\dot{m}_{rod} (L_F + C_p \Delta T) = (\dot{q}_{rod (+)} - \dot{q}_{rod (-)})$, as the rod loses energy to the water layer in addition to heating the fuel layers. Thus, the overall additional mass loss rate reduces for the rod immersed at 50 mm case as shown in Fig. 3.9 (b).

Figure 3.10 (c) shows the calculated mass burning rate for 12 trials across 4 cases (Baseline, 10 mm immersed rod, 30 mm immersed rod, 50 immersed rod), using the energy balance and heat transfer model as described above in Section 3.2, plotted against the experimental burning rate obtained directly from the fuel replenishing system. The red dotted lines indicate a deviation error of $\pm 15\%$. It is seen that the calculated values using the heat transfer model are in good agreement with the experimental values and fall within the error margin of 15%, showing the model works well for the detailed thermal study. Further, Figure 3.10 (d) shows the calculated and experimental mass loss plotted against experimented cases as a function of rod depths. The plot clearly shows that the rod in the optimum location in the hot zone has the highest mass burning rates as explained and the trend has been captured accurately based on the model. Thus, the model gives insight into the heat transfer mechanisms and identifies parameters required for optimal rod depth.

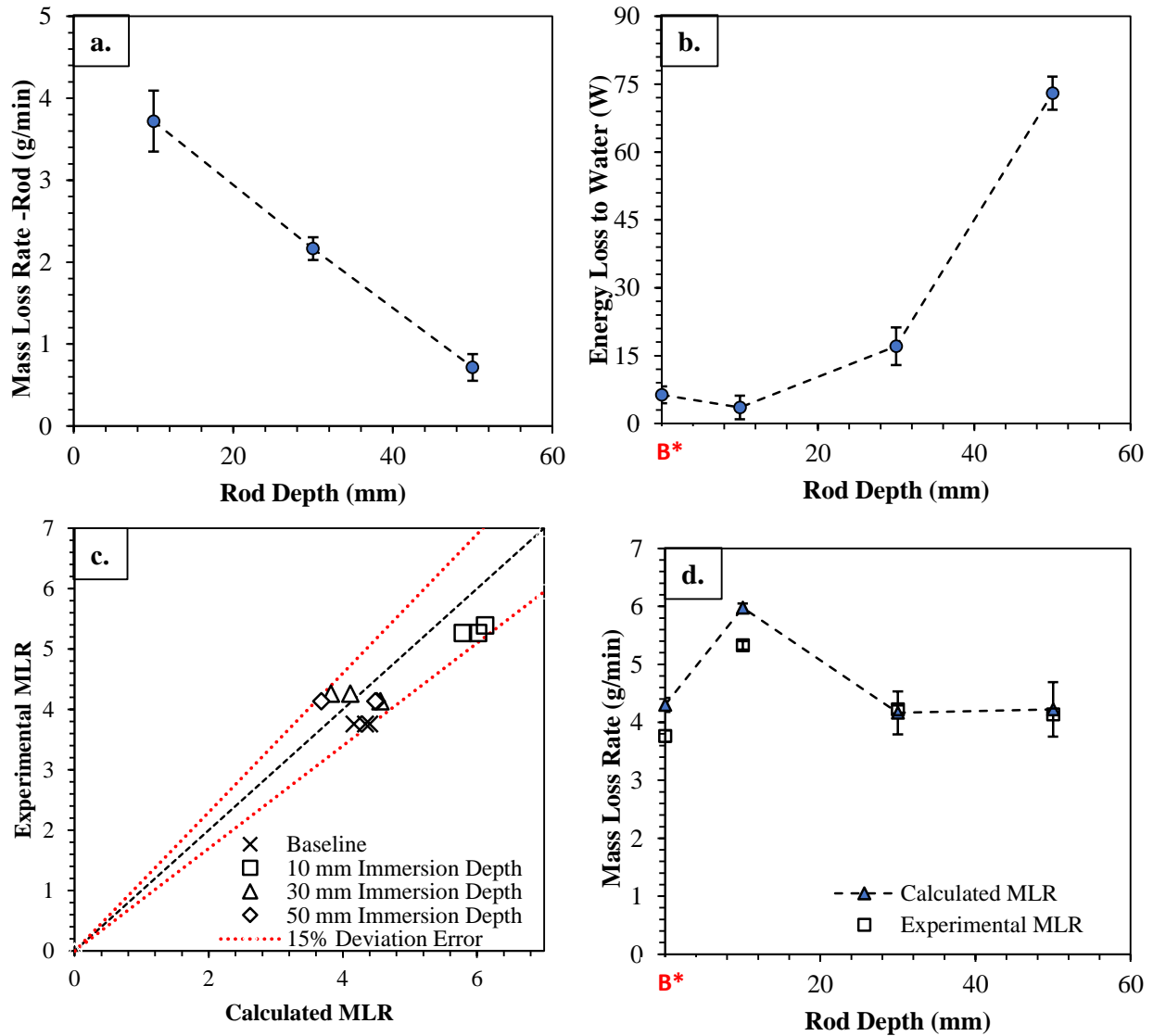


Figure 3.10. Obtained heat transfer model results (a) Energy loss to water sublayer plotted against baseline and three rod depths, (b) Additional mass loss rate due to immersed rod plotted against rod depths, (c) Calculated burning rate from the heat transfer model for 12 trials in comparison to the experimental burning rate obtained directly from the fuel replenishing system for baseline and three immersion depths, (d) Calculated and experimental MLR for baseline and three immersion depths. (B^* denotes baseline case).

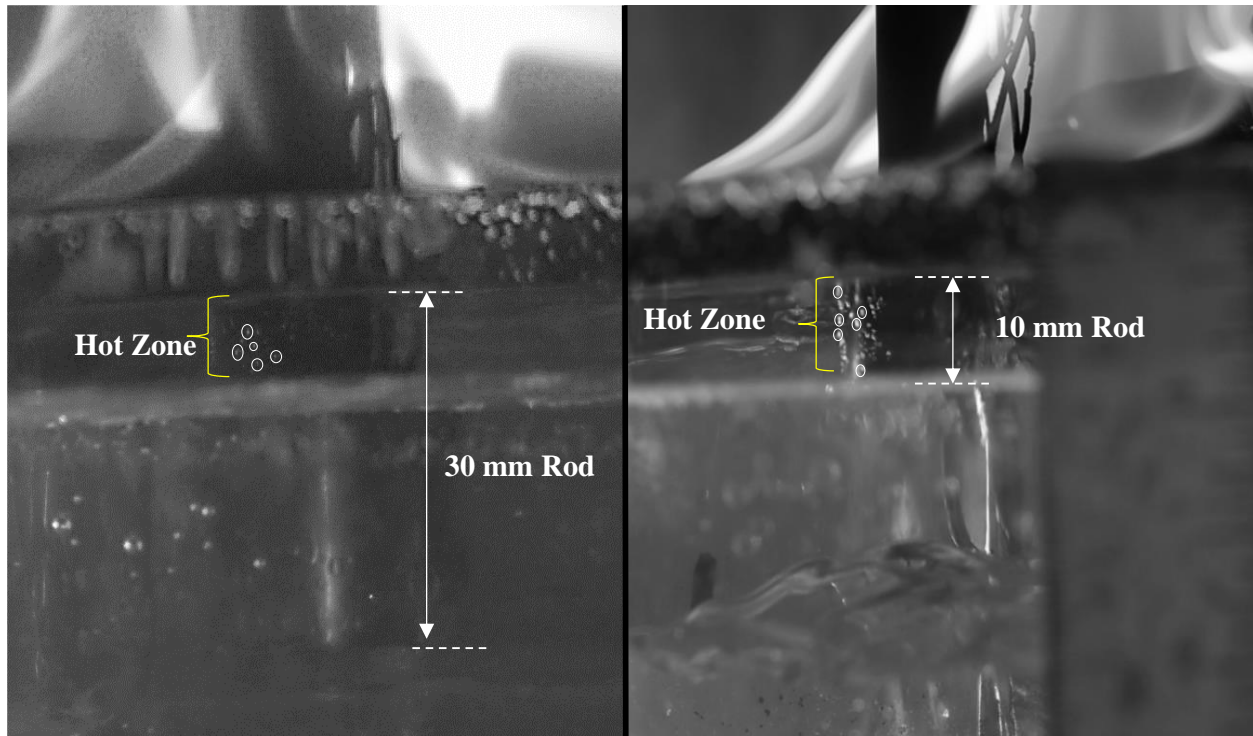


Figure 3.11. Thermal penetration depth (δ) observed indicated by bubbling sites on the rod surface with 30 mm depth and 10 mm rod depth.

3.4. Conclusion

In-situ burning has been identified as an effective countermeasure in oil spill clean-up in water bodies. However, the burning process is quite challenging as the water sublayer acts as a heat sink, thus reducing the oil burning rates and affecting the overall clean-up efficiency. To overcome this reduction in the burning rate due to wavy water conditions, a thermally conductive object is placed in the fire that is immersed in the fuel layer. The burning behavior of a 40 mm floating fuel layer on a turbulent water sublayer ($u' = 1.7$ cm/s) with an immersed copper rod is investigated. The immersion depth of the rod is varied from 5 mm to 50 mm. Results show when the rod is closer to the surface of the fuel surface (5 mm and 10 mm from the fuel surface) in the hot zone, the burning rate of the fuel increases by about 30% as compared to a baseline no-rod case. Thus, even under the action of the wavy water sublayer, the presence of the rod enhances the burning rate. When the copper rod is immersed further (20 mm, 30 mm, 50 mm), the burning rate increases

by about 12.5% as compared to the baseline case. An energy behavior shows that net energy feedback to the fuel from the rod immersed in the fuel layer is higher than the baseline case. Additionally, the heat loss to the water layer has been quantified for the different cases of rod depths. It is seen that as the immersion depth of the rod increases beyond 10 mm, the heat loss to water increases thus reducing the net energy available for the fuel burning. The mass loss rates obtained from the heat transfer model are in close agreement with the experimental mass burning rates and the model provides detailed insight into the heat transfer phenomenon for optimizing the immersed object location in the fuel layer.

Chapter 4: Conclusion and Future Work

In the study, a bench scale experimental platform is developed to analyze quasi-steady burning of fuel slick on a turbulent water sublayer. In a confined Pyrex cylindrical tube, the turbulence is created by using a submerged jet pointing upwards, creating a free bulk flow on the surface at the water. In this confined flow setup, the surface turbulence of the water is directly proportional to flow rate of the pump and this flow rate is controlled using a flow valve for obtaining the desired turbulent intensity. The corresponding turbulence ranges from 0 cm/s to 6.6 cm/s. Experiments are conducted with regressing fuel as well as a steady layer of fuel as seen in Chapter 2 and Chapter 3. Temperature profiles are closely monitored to study the heat transfer mechanism at gas-fuel and fuel-water interfaces.

Chapter 2 evaluates the burning behavior of fuel under the influence of turbulence in two sections. The first section only studies the influence of mass loss rate of the fuel corresponding to changing turbulent intensities. For this section turbulence is varied in increments of 0.8 cm/s until a condition is reached where burning no longer sustains. Results showed a reduction in the burning rate as the turbulence intensity increased. The second section of the chapter analyzes the quasi-steady behavior of the fuel under turbulence intensity 0 cm to 4.2 cm/s. Heat transfer model showed energy available for vaporization decreases with increase in turbulence. Additionally, a model is developed to quantify the heat transfer coefficient at the fuel-water interface. The model predicted an increase in heat transfer coefficient from 40 W/m²-K to about 125 W/m²-K for increasing turbulence intensity validating that the convective heat transfer significantly increases at the interface with turbulence. Thus, this chapter gives a basic understanding of the burning behavior of thin fuel slick subjected to varying turbulence, that can be applied to ISB situations.

From information obtained from Chapter 2, Chapter 3 evaluates the introduction of immersed conductive objects as countermeasure to enhance burning rate of fuel slicks with turbulent water sublayer. For this study, a constant fuel thickness of 40 mm is maintained to study the effect of depth of an immersed copper rod (5mm to 50mm) on the burning behavior of the fuel. Immersion depth of 10 mm is identified as an optimum depth for increasing burn rate. Results showed that as the rod is placed closer to the water, it

loses a significant amount of heat to the water sublayer. Thus, 10 mm immersed copper rod increased the burn rate by 30% from baseline no rod case by preheating and vaporizing the fuel close to the fuel surface. Temperature measurement in the fuel showed a presence of a hot zone that indicates the increases burning for optimized case with 10 mm. A heat transfer model was further used to calculate the energy balance for the fuel layer. A detailed energy budgeting was done to determine the heat input and loss terms during the burning process with a rod. The overall burning rate predicted from the model is in close agreement with experimental values. The error for calculated and experimental values falls within 15%. Thus, this chapter provides an insight to increase the burning behavior with turbulent surface with an identified hot zone and optimized immersion depth for conductive objects. This has direct application on advancing in-situ burning operations by using these immersed objects as the optimum location of the object is based on the hot zone of the fuel.

The current study shows insights of turbulence as a changing parameter and its consequent effects, this can be beneficial for ISB burns to understand basic heat transfer for varying turbulence. The Flame RefluxerTM technology with immersed conductive objects can be a solution for faster and cleaner burns. Although, the current experimental matrix chooses only a single rod, the experimental setup and the heat transfer analysis can be extended to studies pertaining to multiple rods. A coupled effect of multiple immersed objects on the burning behavior is envisioned in a future study enabling additional enhancement in the burning rates of fuel slicks in wavy waters.

References

1. IEA. 2021. Daily demand for crude oil worldwide from 2006 to 2020, with a forecast until 2026* (in million barrels per day). Statista. Statista Inc. Accessed: December 08, 2022. <https://www.statista.com/statistics/271823/daily-global-crude-oil-demand-since-2006/>
2. <https://storymaps.arcgis.com/stories/c469a794e6be48049ee0e29f23ca2038>
3. <https://www.theguardian.com/environment/2022/mar/07/oil-spill-at-sea-who-will-pay-peru-worst-environmental-disaster>
4. Thompson, C.H., Dawson, G.W. and Goodier, J.L., 1979. *Combustion: An oil spill mitigation tool* (No. PNL-2929 Final Rpt.).
5. Goodier, J.L. and Siclari, R.J., 1981. *Combustion: an oil spill mitigation tool. Phase II. The burning of the M/T BURMAH AGATE (ex-DANALAND)* (No. DOE/TIC-11471). Pacific Northwest Lab., Richland, WA (USA).
6. Buist, I., McCourt, J., Potter, S., Ross, S. and Trudel, K., 1999. In situ burning. *Pure and Applied Chemistry*, 71(1), pp.43-65. 266
7. Potter, S. and Buist, I., 2008. In-situ burning for oil spills in arctic waters: State-of-the-art and future research needs. In *Oil Spill Response: A Global Perspective* (pp. 23-39). 268 Springer Netherlands. 269
8. Evans, D.D., Mulholland, G.W., Baum, H.R., Walton, W.D. and McGrattan, K.B., 2001. In situ burning of oil spills. *Journal of research of the National Institute of Standards and Technology*, 106(1), p.231. 272
9. Buist, I., McCourt, J., Potter, S., Ross, S. and Trudel, K., 1999. In situ burning. *Pure and Applied Chemistry*, 71(1), pp.43-65. <https://doi.org/10.1351/pac199971010043>.
10. Teal, J.M. and Howarth, R.W., 1984. Oil spill studies: a review of ecological effects. *Environmental Management*, 8(1), pp.27-43. <https://doi.org/10.1007/BF01867871>.

11. Buist, I. A., “Window of Opportunity for *In Situ* Burning”, *In Situ Burning of Oil Spills Workshop Proceedings*, 21-26, (1998).
12. Arai, M., K. Saito, and R. A. Altenkirch, “Experimental Studies of Burning Liquid Fuels On Water Sub-layer”, *Symposium (International) On Combustion*, 22nd, Seattle, WA, 1-1 pp, (1988).
13. Arai, M., Saito, K. and Altenkirch, R.A., 1990. A study of boilover in liquid pool fires supported on water part I: effects of a water sublayer on pool fires. *Combustion Science and Technology*, 71(1-3), pp.25-40. <https://doi.org/10.1080/00102209008951622>.
14. Garo, J.P. and Vantelon, J.P., 1999. Thin layer boilover of pure or multicomponent fuels. In *Prevention of hazardous Fires and Explosions* (pp. 167-182). Springer, Dordrecht. https://doi.org/10.1007/978-94-011-4712-5_13.
15. Koseki, H. and Mulholland, G.W. (1991) The effect of diameter on the burning of crude oil pool fires. *Fire Technol.*, 27(1), 54–65.
16. Koseki, H., Kokkala, M., and Mulholland, G.W. (1991) Experimental study of boilover in crude oil fires. *Fire Safety Science-Proceedings of the Third International Symposium*. Elsevier, London and New-York, pp. 865–874.
17. Garo, J.P., Gillard, P., Vantelon, J.P. and Fernandez-Pello, A.C., 1999. Combustion of liquid fuels spilled on water. Prediction of time to start of boilover. *Combustion science and technology*, 147(1-6), pp.39-59. 147(1-6), 39-59. <https://doi.org/10.1080/00102209908924211>.
18. Garo, J.P., Vantelon, J.P. and Fernande-Pello, A.C., 1996, January. Effect of the fuel boiling point on the boilover burning of liquid fuels spilled on water. In *Symposium (International) on Combustion* (Vol. 26, No. 1, pp. 1461-1467). Elsevier. [https://doi.org/10.1016/S0082-0784\(96\)80367-5](https://doi.org/10.1016/S0082-0784(96)80367-5).
19. Garo, J.P., Vantelon, J.P. and Fernandez-Pello, A.C., 1994, January. Boilover burning of oil spilled on water. In *Symposium (International) on Combustion* (Vol. 25, No. 1, pp. 300 1481-1488). Elsevier. [https://doi.org/10.1016/S0082-0784\(06\)80792-7](https://doi.org/10.1016/S0082-0784(06)80792-7).

20. Garo, J.P., Vantelon, J.P. and Koseki, H., 2006. Thin-layer boilover: Prediction of its onset and intensity. *Combustion science and technology*, 178(7), pp.1217-1235. <https://doi.org/10.1080/00102200500296846>.
21. Arai, M., Saito, K. and Altenkirch, R.A., 1990. A study of boilover in liquid pool fires supported on water part I: effects of a water sublayer on pool fires. *Combustion Science and Technology*, 71(1-3), pp.25-40. <https://doi.org/10.1080/00102209008951622>.
22. Ito, A., Saito, K. and Inamura, T., 1992. Holographic interferometry temperature measurements in liquids for pool fires supported on water.
23. Inamura, T., Saito, K. and Tagavi, K.A., 1992. A study of boilover in liquid pool fires supported on water. Part II: Effects of in-depth radiation absorption. *Combustion science and technology*, 86(1-6), pp.105-119.
24. Van Gelderen, L., Brogaard, N.L., Sørensen, M.X., Fritt-Rasmussen, J., Rangwala, A.S. and Jomaas, G., 2015. Importance of the slick thickness for effective in-situ burning of crude oil. *Fire Safety Journal*, 78, pp.1-9.
25. Van Gelderen, L., Malmquist, L.M.V., Jomaas, G., 2017. Vaporization order and burning efficiency of crude oils during in-situ burning on water. *Fuel* 191, 528–537. <https://doi.org/10.1016/J.FUEL.2016.11.109>.
26. Kong, D., He, X., Yang, H., Zhang, Z., 2019. Experimental study for flame base drag and burning efficiency of spilled crude oil during in-situ burning on water. *Process Saf. Environ. Prot.* 131, 48–54.
27. Sauer, N.G., Cuendet, J.M. and Rangwala, A.S., 2022. A study of thin fuel slick combustion on wavy water. *Marine Pollution Bulletin*, 182, p.113932.
28. Sauer, N.G., M. Kottalgi, K.S. Arsava, and A.S. Rangwala, Burning Behaviour of an Oil Slick with Waves, Proceedings of the Forty-third AMOP Technical Seminar, Environment and Climate Change Canada, Ottawa, ON, Canada, pp. 49-56, 2021.
29. Chang, L. and Rangwala, A.S., 2022. Experimental study of crude oil slick burning on a turbulent water surface. *Combustion and Flame*, 241, p.112119. <https://doi.org/10.1016/j.combustflame.2022.112119>.

30. Aurell, J., Holder, A., Gullett, B., Lamie, N., Arsava, K., Conmy, R., Sundaravadivelu, D., Mitchell, W., Stone, K., 2021. Analysis of emissions and residue from methods to improve efficiency of at-sea, in situ oil spill burns. *Mar. Pollut. Bull.* 173 <https://doi.org/10.1016/J.MARPOLBUL.2021.113016>.
31. Rangwala, A. S, Arsava, K. S, Mahnken .G, Xiaochuan .S. 2015. A novel experimental approach to enhance burning of oil-water emulsions by immersed objects (*Final Report, Department of Fire Protection Engineering, Worcester Polytechnic Institute*). <https://www.bsee.gov/sites/bsee.gov/files/osrr-oil-spill-response-research/1049aa.pdf>
32. Rangwala, A. S., Shi, X., Arsava, K. S., & Mahnken, G, 2017. U.S. Patent No. 9,772,108. Washington, DC: *U.S. Patent and Trademark Office*.
33. Arsava, K. S., Raghavan, V., & Rangwala, A. S. 2018. Enhanced oil spill clean-up using immersed thermally conductive objects. *Fire Technology*, 54(6), 1745-1758. <https://doi.org/10.1007/s10694-018-0767-2>.
34. Arsava, K. S., Rangwala, A. S, Hansen. K., 2017. An offshore in-situ burn enhanced by immersed objects, *40th AMOP Tech. Semin. Environ. Contam. Response*.
35. Nair, S., Mahnken, G., Arsava, K.S. and Rangwala, A.S., 2022. Modeling the Influence of Immersed Objects on Pool Fire Burning. *Fire Technology*, pp.1-25. <https://doi.org/10.1007/s10694-022-01233-2>.
36. Pi, X., Chang, L. and Rangwala, A.S., 2021. The burning rate of a pool fire increased by bubble behaviors during nucleate boiling. *Fire Safety Journal*, 120, p.103097. <https://doi.org/10.1016/j.firesaf.2020.103097>.
37. Sezer, H., Arsava, K.S. and Rangwala, A.S., 2017. Oil spill clean-up using immersed metal wool. *Journal of environmental chemical engineering*, 5(5), pp.5196-5206. <https://doi.org/10.1016/j.jece.2017.09.052>.
38. Sezer, H., Arsava, K.S., Kozhumal, S.P. and Rangwala, A.S., 2017. The effect of embedded objects on pool fire burning behavior. *International Journal of Heat and Mass Transfer*, 108, pp.537-548. <https://doi.org/10.1016/j.ijheatmasstransfer.2016.12.021>.

39. Gargett, A.E., 1989. Ocean turbulence. *Annual Review of Fluid Mechanics*, 21(1), pp.419-451.
40. Sonin, A.A., Shimko, M.A. and Jung-Hoon, C., 1986. Vapor condensation onto a turbulent liquid—I. The steady condensation rate as a function of liquid-side turbulence. *International journal of heat and mass transfer*, 29(9), pp.1319-1332.
41. Brown, J.S., Khoo, B.C. and Sonin, A.A., 1990. Rate correlation for condensation of pure vapor on turbulent, subcooled liquid. *International journal of heat and mass transfer*, 33(9), pp.2001-2018.
42. Khoo, B.C., Chew, T.C., Heng, P.S. and Kong, H.K., 1992. Turbulence characterisation of a confined jet using PIV. *Experiments in fluids*, 13, pp.350-356.
43. Hu, W.K., 1993. Particle ejection and suspension due to isotropic turbulence (Doctoral dissertation, Massachusetts Institute of Technology).
44. Morse, T.L. and Kytömaa, H.K., 2011. The effect of turbulence on the rate of evaporation of LNG on water. *Journal of loss prevention in the process industries*, 24(6), pp.791-797.
45. Barchilon, M. and Curtet, R., 1964. Some details of the structure of an axisymmetric confined jet with backflow. <https://doi.org/10.1115/1.3655953>.
46. National Center for Biotechnology Information (2023). PubChem Compound Summary for CID 8182, Dodecane. Retrieved February 7, 2023 from <https://pubchem.ncbi.nlm.nih.gov/compound/Dodecane>.
47. Shi, X., Bellino, P.W., Simeoni, A. and Rangwala, A.S., 2016. Experimental study of burning behavior of large-scale crude oil fires in ice cavities. *Fire Safety Journal*, 79, pp.91-99.
48. Quintiere, J.G., 2006. *Fundamentals of fire phenomena*.
49. Planas-Cuchi, E., Chatris, J.M., López, C. and Arnaldos, J., 2003. Determination of flame emissivity in hydrocarbon pool fires using infrared thermography. *Fire Technology*, 39, pp.261-273.
50. Farahani, H.F., Jomaas, G. and Rangwala, A.S., 2015. Effects of convective motion in n-octane pool fires in an ice cavity. *Combustion and Flame*, 162(12), pp.4643-4648.
51. Zhao, J., Huang, H., Jomaas, G., Zhong, M. and Yang, R., 2018. Experimental study of the burning behaviors of thin-layer pool fires. *Combustion and Flame*, 193, pp.327-334.

52. Steckler, K.D., Kashiwagi, T., Baum, H.R. and Kanemaru, K., 2006, February. Analytical model for transient gasification of noncharring thermoplastic materials. In *Fire Safety Science—Proceedings of the Third International Symposium* (pp. 895-904). Routledge. <https://doi.org/10.3801/iafss.fss.3-895>
53. Wicks III, M., 1969. Fluid dynamics of floating oil containment by mechanical barriers in the presence of water currents. In *International Oil Spill Conference* (Vol. 1969, No. 1, pp. 55-106). American Petroleum Institute.